

## Journal Pre-proofs

Tracing acid mine drainage and estuarine Zn attenuation using Cd and Zn isotopes

Hollie Packman, Susan H. Little, José Miguel Nieto, M. Dolores Basallote, Rafael Pérez-López, Barry Coles, Katharina Kreissig, Tina van de Flierdt, Mark Rehkämper

PII: S0016-7037(23)00432-5  
DOI: <https://doi.org/10.1016/j.gca.2023.09.001>  
Reference: GCA 13157

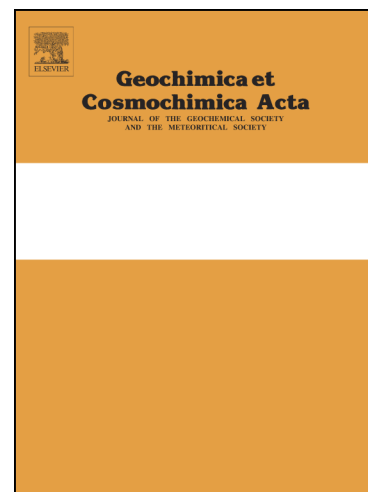
To appear in: *Geochimica et Cosmochimica Acta*

Received Date: 17 March 2023  
Accepted Date: 5 September 2023

Please cite this article as: Packman, H., Little, S.H., Miguel Nieto, J., Dolores Basallote, M., Pérez-López, R., Coles, B., Kreissig, K., van de Flierdt, T., Rehkämper, M., Tracing acid mine drainage and estuarine Zn attenuation using Cd and Zn isotopes, *Geochimica et Cosmochimica Acta* (2023), doi: <https://doi.org/10.1016/j.gca.2023.09.001>

This is a PDF file of an article that has undergone enhancements after acceptance, such as the addition of a cover page and metadata, and formatting for readability, but it is not yet the definitive version of record. This version will undergo additional copyediting, typesetting and review before it is published in its final form, but we are providing this version to give early visibility of the article. Please note that, during the production process, errors may be discovered which could affect the content, and all legal disclaimers that apply to the journal pertain.

© 2023 Published by Elsevier Ltd.



# Tracing acid mine drainage and estuarine Zn attenuation using Cd and Zn isotopes

Hollie Packman<sup>a,b</sup>, Susan H. Little<sup>b,c,\*</sup>, José Miguel Nieto<sup>d</sup>, M. Dolores Basallote<sup>d</sup>, Rafael Pérez-López<sup>d</sup>, Barry Coles<sup>b</sup>, Katharina Kreissig<sup>b</sup>, Tina van de Flierdt<sup>b</sup>, Mark Rehkämper<sup>b</sup>

<sup>a</sup>Science and Solutions for a Changing Planet Doctoral Training Partnership, Grantham Institute - Climate Change and the Environment, Imperial College London, Exhibition Road, South Kensington, London SW7 2AZ, UK

<sup>b</sup>Department of Earth Science and Engineering, Imperial College London, South Kensington Campus, London SW7 2AZ, UK

<sup>c</sup>Department of Earth Sciences, University College London, Gower Street, London WC1E 6BT, UK

<sup>d</sup>Department of Earth Sciences & Research Center on Natural Resources, Health and the Environment, University of Huelva, Campus 'El Carmen', 21071 Huelva, Spain

\*Corresponding author: [susan.little@ucl.ac.uk](mailto:susan.little@ucl.ac.uk)

Keywords: Acid Mine Drainage, Cd isotopes, Zn isotopes, Estuary, Metal isotope fingerprint

It has been estimated that the acid mine drainage (AMD) impacted Odiel river basin in southern Spain supplies 0.37% and 15% of the global riverine fluxes of Cd and Zn to the oceans, respectively (Sarmiento et al., 2009). However, the behaviour of Cd and Zn in the Ria of Huelva estuary, which connects the Odiel and Tinto watersheds with the Gulf of Cadiz, has yet to be fully investigated. Furthermore, very few studies have investigated Cd and Zn isotope behaviour in estuaries worldwide. This study presents Cd and Zn concentrations and isotopic compositions for the Ria of Huelva estuary and surrounding watersheds, sampled in 2017 and 2019. Sulfide-rich rock samples extracted from three mines yield Cd and Zn isotope compositions that range from  $-0.14\text{‰}$  to  $+0.07\text{‰}$  ( $n = 4$ ) for  $\delta^{114}\text{Cd}$  and  $-0.01\text{‰}$  to  $+0.29\text{‰}$  ( $n = 4$ ) for  $\delta^{66}\text{Zn}$ . However, a uniform riverine signal of about  $+0.02\text{‰}$  for Cd and  $+0.17\text{‰}$  for Zn indicates that tracing of individual mining regions using Cd and Zn isotopes is challenging. Limited variability was observed in dissolved  $\delta^{114}\text{Cd}$  values throughout the watershed, including AMD, the estuary, and the Gulf of Cadiz, with a mean value of  $\pm 0.00 \pm 0.13\text{‰}$  ( $n = 25$ , 2 SD; excludes one AMD outlier, at  $+0.48\text{‰}$ ), including both 2017 and 2019 data. By contrast,  $\delta^{66}\text{Zn}$  values ranged from  $-0.12\text{‰}$  to  $+0.35\text{‰}$  ( $n = 28$ ) for the same geographical and temporal scope. In May 2017, a large spill from an abandoned mine, La Zarza, resulted in a drastic increase in the concentrations of trace metals reaching the estuary compared to 2019, but no impact of this mine spill on Cd or Zn isotope compositions is observed. In 2019, an increase in  $\delta^{66}\text{Zn}$  values in the estuary coincided with high pH values (up to  $\text{pH} = 8.8$ ) and chloride concentrations (2.73%), which may reflect an alkaline anthropogenic input from the active neighbouring industrial complex. Overall, Cd concentrations and isotope compositions in the estuary are largely consistent with conservative mixing behaviour. By contrast, Zn behaviour is non-conservative, with removal of 49 to 97% of dissolved riverine Zn in the estuary during the period 2017 to 2019, associated with a relatively small isotopic shift to lighter Zn isotope compositions. Removal of Zn to the particulate phase in the Ria of Huelva estuary therefore largely attenuates high riverine Zn fluxes from AMD, indicating that previously estimated Odiel river basin Zn fluxes were overestimated. Nevertheless, the variable but generally light AMD Cd and Zn isotope compositions, coupled with high dissolved metal concentrations, suggest that Cd and Zn isotopes may be useful tracers of regionally averaged AMD inputs to the Gulf of Cadiz and beyond.

The trace elements Cd and Zn have important biological roles as cofactors in enzymes (Morel and Price, 2003; Bruland et al., 2013; Twining and Baines, 2013), but are toxic at higher concentrations (e.g., Vig et al., 2003; Muysen et al., 2006; de Paiva Magalhães et al., 2015). Toxicity and bioaccumulation in biota is particularly marked for Cd, with significant enrichments of Cd in soil and aquatic systems deriving from various anthropogenic activities (e.g., Spehar et al., 1978; Vig et al., 2003; Wright and Welbourn, 2011). Hence, considerable research has been dedicated to understanding the respective biogeochemical cycles of Cd and Zn (e.g., Morel and Price, 2003; Rauch and Pacyna, 2009; Cullen and Maldonado, 2013; Araújo et al., 2017; Horner et al., 2021). Coupling the analysis of Cd and Zn concentrations and their isotope compositions offers distinct advantages over concentration analyses alone. For example, distinct sources of Cd and Zn may be identified and quantified (Yin et al., 2016; Araújo et al., 2017; Desaulty and Petelet-Giraud, 2020; Yin et al., 2021; Araújo et al., 2022; Fang et al., 2022). Alternatively, pathways of metal transfer may be discernible, because biogeochemical processes (e.g., adsorption, complexation, biological uptake) result in stable isotope fractionation (e.g., Pokrovsky et al., 2005; Gélabert et al., 2006; John et al., 2007; Balistrieri et al., 2008; Juillot et al., 2008; Jouvin et al., 2009; Horner et al., 2011; Wanty et al., 2013; Wasylenki et al., 2014; Bryan et al., 2015; Dong and Wasylenki, 2016; Gou et al., 2018; Mavromatis et al., 2019; Wang et al., 2023). Thus, the isotopic systems of Cd and Zn aid in evaluating their biogeochemical cycling (e.g., Ripperger et al., 2007; Conway and John, 2014; John and Conway, 2014; Zhao et al., 2014; Little et al., 2014; Wiederhold, 2015; Roshan et al., 2018; John et al., 2018; Desaulty and Petelet-Giraud, 2020; Araújo et al., 2022).

Cadmium and Zn are mobilised from natural origins, e.g., continental rocks (Chester and Jickells, 2012; Cullen and Maldonado, 2013; Little et al., 2014), but also through anthropogenic processes (Pacyna and Pacyna, 2001). Acid mine drainage (AMD) is a significant anthropogenic source of trace metals to the environment and a major environmental problem. It is estimated that 19,300 km of rivers and 72,000 ha of water bodies were affected by AMD in the USA in 1989 (Johnson and Hallberg, 2005). AMD is generated by the oxidation of sulfide minerals such as pyrite ( $\text{FeS}_2$ ), chalcopyrite ( $\text{CuFeS}_2$ ) and sphalerite ( $\text{ZnS}$ ) (Plumlee et al., 2020). The interaction of sulfide minerals with oxygen, water and microorganisms (Singer and Strumm, 1970) results in acidic, highly concentrated wastewater of dissolved metal sulfates and soluble salts (Buckby et al., 2003; Plumlee et al., 2020). Oxidative dissolution of sulfide minerals occurs naturally ('sulfide weathering') but is accelerated many-fold at mining sites due to enhanced exposure of primary sulfide minerals. Further, the production of AMD can continue for many years after active mining has ceased (Johnson and Hallberg, 2005; Sarmiento et al., 2009). The oxidation rate is dependent on the generation of ferric iron from ferrous iron, which can be catalysed by acidophilic bacteria (e.g., *Acidithiobacillus ferrooxidans*). In the presence of such bacteria, the rate of pyrite dissolution can increase by  $\times 10^6$  (Singer and Strumm, 1970). Bioleaching of sulfide minerals often occurs in extreme conditions, yet, there is a large diversity of microorganisms that survive the polymetallic mining environment and catalyse the leaching, including heterotrophic bacteria and fungi (Edwards et al., 1999; Asghari et al., 2013; Pattanaik et al., 2020).

The Iberian Pyrite Belt is one of the largest metallogenetic massive sulfide regions in the world, with original reserves estimated to have contained >1700 Mt of sulfide ores (Leistel et al., 1997). The local watershed is severely affected by AMD, whereby extreme Fe concentrations colour large sections of the Odiel and Tinto Rivers red. Indications suggest mining in the region began in the third millennium BCE (Nocete et al., 2005), with extraction later scaled up by the Romans. It is estimated that 25 Mt of sulfide ore was mined in the 4<sup>th</sup> Century (Strauss et al., 1977). The mining effluents from active and abandoned mines today result in dissolved trace metal (e.g., Zn, Cd, Cu) concentrations in the Odiel and Tinto Rivers a factor of  $\times 10^6$  higher than their respective concentrations in uncontaminated streams (Van Geen et al., 1997; Gaillardet et al., 2003; España et al., 2005a). The trace metal-rich waters that drain the metalliferous mining area are transported to the Gulf of Cadiz and onwards to the western Mediterranean Sea (e.g., Elbaz-Poulichet et al., 2001) and eastern Atlantic (Laiz et al., 2020). Estimates suggest the flux of trace metals discharging from the Odiel and Tinto Rivers could account for 0.37% and 15% of the total global riverine dissolved flux of Cd and Zn, respectively (Sarmiento et al., 2009). However, before discharging into the Gulf of Cadiz the trace metals from the Odiel and Tinto Rivers pass through the Ria of Huelva estuary, where their behaviour is not well constrained.

Endeavours aimed at further understanding the mechanisms controlling the behaviour of trace metals in estuaries are important for riverine flux and marine mass balance calculations, and in understanding coastal biogeochemical cycles. Estuaries contain strong hydrochemical gradients in salinity, density, flow velocity and pH (Elliott and McLusky, 2002). In general, dense saltwater intrusion occurs along the bottom of an

estuary with buoyant freshwater above, creating a so-called 'estuarine circulation'. The zone in which the two

1969; Burchard et al., 2018). Strong turbidity gradients in estuaries may encourage intense adsorption of Cd and Zn onto particulates from the dissolved phase at the maximum turbidity zone (Petit et al., 2015; de Souza Machado et al., 2016). Thereafter, increasing salinity introduces seawater cations that compete for adsorption sites and can induce desorption of Cd and Zn (Paalman et al., 1994; Fairbrother et al., 2007). As a result, estuarine behaviour of Cd and Zn can be complex and non-conservative, though Cd is typically more conservative than Zn because of the formation of Cd *chloro*-complexes at  $\text{pH} > 7$  (Elbaz-Poulichet et al., 1987; Shiller and Boyle, 1991; Paalman et al., 1994; Dai and Martin, 1995; Dabrin et al., 2009; Cánovas et al., 2020). For typical estuaries, the salinity gradient is the controlling factor for geochemical processes, but for estuaries affected by AMD, such as the Ria of Huelva estuary, the large pH increase is also an important variable.

This work examines Cd and Zn concentrations and isotopic compositions in AMD influenced samples from southern Spain. The focus is on dissolved and particulate phase sampling in the Ria of Huelva estuary, which connects the Tinto and Odiel Rivers to the Gulf of Cadiz (Figure 1). Massive sulfide deposits from three different mines were also analysed, encompassing both volcanic and sedimentary-hosted mineralisation, alongside proximal river water samples, to assess the impact of geology on the riverine and estuarine dissolved phase compositions. Finally, coastal surface seawater samples from the Gulf of Cadiz were examined to investigate the downstream impacts of regional AMD on the coastal ocean.

This study aims to examine the following five questions: (1) What is the role of the local geology in determining the isotopic fingerprint of AMD? (2) How do biogeochemical processes in the river and estuary modify this fingerprint? (3) Can Cd and/or Zn be used to fingerprint other (non-AMD) anthropogenic sources of trace metals to the estuary? (4) What is the flux of metals to the Gulf of Cadiz and, ultimately, the Atlantic Ocean, and are these fluxes significantly reduced due to estuarine removal processes? (5) Can Cd or Zn isotope ratios be used as a tracer of AMD, either locally or regionally?

## 2. Sampling and methods

### 2.1 Site description

The Iberian Pyrite Belt (IPB) extends from Seville in southwest Spain to the Atlantic coast in Portugal, south of Lisbon. It is 250 km long and 30 km wide and forms part of the South Portuguese Zone of the Hercynian Iberian Massif (Sáez et al., 1999). The IPB contains a vast number of massive sulfide deposits with large metal reserves, from which metals such as Au, Ag and Cu have been extracted for approximately 4500 years (Sáez et al., 1999; Nocete et al., 2005).

The IPB has been sub-divided geographically and in relation to the types of mineralisation present (Sáez et al., 1999; Tornos et al., 2008). The northern zone of the belt (including the San Telmo mine) is characterised by massive sulfides hosted in pumice-rich volcanoclastic rocks. Deposits in this region are generally thought to have formed by the replacement of the volcanic rocks (Tornos, 2006). The southern zone (including the Tharsis mine) contains predominantly volcano-sedimentary-hosted (including black shale) pyrite-rich deposits. These deposits are thought to be exhalative, forming in marine basins by brine accumulation and biogenic activity. The Rio Tinto mining district (including the Corta Atalaya mine), historically one of the most important districts, is in the middle zone of the IPB, which has been described as intermediate between the northern and southern deposits (Tornos et al., 2008).

The Tinto and Odiel Rivers flow through densely compacted massive polymetallic sulfide deposits and mining wastes in the Huelva province. The main minerals in these deposits and wastes are pyrite ( $\text{FeS}_2$ ), sphalerite ( $\text{ZnS}$ ), galena ( $\text{PbS}$ ), chalcocite ( $\text{Cu}_2\text{S}$ ), arsenopyrite ( $\text{FeAsS}$ ) and other sulfides (Sarmiento et al., 2009). The Odiel River (Río Odiel) is 140 km long and drains an area of 2300 km<sup>2</sup> with tributaries that have a length of 1149 km (Sarmiento et al., 2009; Nieto et al., 2013). The Tinto River (Río Tinto) is 100 km long with a surface watershed spanning 720 km<sup>2</sup> (Nieto et al., 2013). Both rivers converge at a coastal wetland known as the Ria of Huelva. The Ria of Huelva estuary is a mesotidal, semi-diurnal, bar-built estuary (Borrego et al., 1995), with a mean amplitude of 2.5 m, in which seawater from the Gulf of Cadiz meets highly concentrated and acidic freshwaters from the Odiel and Tinto basins. Parts of the estuary, as well as the Tinto and Odiel Rivers, are included in the Natura 2000 network of nature protection areas of the European Union (Olías et al., 2004).

the Huelva region produces long periods of drought, which generate evaporitic sulfate salts (Buckby et al., 2003). Short but intense rainfall events redissolve these salts, known as first flush (or wash-out), creating watercourses that are highly acidic and concentrated in trace metals (Gzyl and Banks, 2007; Cánovas et al., 2010). Hence, rainfall and flood events greatly impact the chemistry of the rivers.

In addition to the extensive impact of AMD in the Huelva Province, the region also has about 500,000 inhabitants and features intensive agriculture and large industries, including mining, pyrometallurgy and phosphogypsum storage. About 100 Mt of phosphogypsum waste is stored in stacks on the salt marshes of the Ria of Huelva estuary. Phosphogypsum is a by-product from the production of phosphoric acid fertilizer and formed by wet chemical attack of phosphate ores with sulfuric acid. It is mainly composed of gypsum but also harbours  $H_3PO_4$  as well as radionuclides and heavy metals as impurities (Martin et al., 2001; Rentería-Villalobos et al., 2010). Cadmium is the most enriched trace metal in phosphate rock, the precursor to phosphogypsum (Martin et al., 2001), and a significant source of Cd to the Ria of Huelva has previously been identified linked to discharge from the phosphogypsum stacks (Pérez-López et al., 2016).

## 2.2 Sampling

To investigate the impact of flood events on the estuary and Gulf of Cadiz, water samples in this study were collected immediately following a significant spill from the abandoned La Zarza mine in May 2017 (Olías et al., 2019). To investigate the recovery and longer-term impacts of the spill, further samples in the estuary and the Gulf of Cadiz were collected in 2018 and 2019. To characterise the baseline geology and freshwater inputs to the estuary, a limited number of river water and mine sulfide rock samples were collected in 2019 (Figure 1).

In detail, two sampling campaigns for dissolved and particulate phase isotopic analyses were carried out in May 2017 and June 2019; these samples are the primary focus of this study. Further sampling campaigns were carried out in March, May, and November 2018 for concentration analyses only (Supplementary Text; Figure S1). In the first campaign in May 2017, six water samples were collected from a boat along the Odiel branch of the Ria of Huelva estuary and the confluence, as well as four samples from the Gulf of Cadiz. In June 2019 the sampling locations followed a similar trajectory, with sampling at the same four localities in the Gulf of Cadiz and similar localities along the Odiel branch of the estuary (Figure 1). Further, two samples were collected along the Tinto branch of the estuary (TRX and TR9). TRX was chosen for its proximity to the large phosphogypsum stacks stored on the salt marshes near Huelva, and an aliquot of the 'process water' (PW) that sits on top of these stacks was also obtained for analysis. Notably, climatic conditions during sampling in 2019 were very dry (0.1 mm rainfall in June 2019) compared to 2017 (21 mm rainfall in May 2017) (Zepner et al., 2021).

For sampling, a Van Dorn water sampler was lowered to the half depth of the estuary (of about 7 m) to avoid boat emissions. A small sample aliquot was decanted and filtered through a syringe filter for the determination of standard physicochemical parameters, including temperature, pH, conductivity, and oxidation-reduction potential (ORP) in the field using HANNA HI98190 and 98192 portable meters. A three-point calibration was performed for both EC (147  $\mu S/cm$ , 1413  $\mu S/cm$ , and 12.88 mS/cm) and pH (4.01, 7.00, and 9.21), while the ORP was controlled using two points (240 and 470 mV). Estuarine and seawater samples for isotope analyses were collected in acid-cleaned 0.25–1 L HDPE bottles for further processing in the laboratory.

Four river water samples were obtained in 2019 (Figure 1). Two of these samples were collected near the source of the Tinto River and the Rio Tinto mine district, including Corta Atalaya mine (TR1 and TR2). Sample TR2 was collected from a stream strongly influenced by AMD originating from the Rio Tinto mine district, signified by its dark red colour (Figure 2). Sample TR1 was collected upstream of the inflow of the AMD-influenced tributary. Hence, TR1 should represent something closer to 'natural background' sulfide weathering. It is orange in colour, likely due to the formation of the mineral schwertmannite (Figure 2). A third sample was collected approximately 18 km downstream, from the main stem of the Tinto River (TR3). A final freshwater sample was collected from a tributary leading to the Odiel River, which is strongly influenced by discharge from the Tharsis mine (THdis).

Finally, the sample set includes four sulfide rock samples from three mines in the region, encompassing the range of IPB mineralisation types: two black shale-hosted sulfide samples from the Tharsis mine (southern zone, TH1, TH2), a volcanic-hosted massive sulfide ore from Corta Atalaya mine (middle zone, CA) and a further volcanic-hosted massive sulfide from San Telmo mine (northern zone, ST).

Estuarine and seawater samples were vacuum filtered through acid-cleaned Whatman cellulose membrane filters (0.22  $\mu\text{m}$ , 47 mm) in 2017, and Sartorius polyamide membrane filters (0.2  $\mu\text{m}$ , 47 mm) in 2019, at the Environmental Mineralogy and Geochemistry Group laboratories, University of Huelva. The filtration rig was thoroughly rinsed with deionised water and pre-conditioned with  $\sim 100$  mL of sample prior to collection in acid-cleaned polyethylene bottles. Samples were then acidified with 1% by volume of suprapur HCl 30% to pH 1.5–2. Particulate and dissolved phase samples were stored in the dark, at  $<4$  °C.

Further analytical work was carried out in the MAGIC Laboratories at Imperial College London. Deionised water of 18.2 M $\Omega$  cm quality from a Milli-Q (MQ) system (Merck Millipore) was used throughout. Acids (HNO<sub>3</sub>, HCl, CH<sub>3</sub>COOH, HF) and 30% H<sub>2</sub>O<sub>2</sub> used in sample preparation were either Optima grade or distilled in Teflon or quartz stills. Nobias Chelate PA1 resin was acquired from Hitachi High-Technologies, Japan. AG MP-1M resin (100-200 mesh), AG1 X8 (200-400 mesh) resin and Eichrom TRU resin were purchased from Bio-Rad Laboratories Ltd. Ammonium hydroxide was purified by cold ammonia-water vapour-liquid equilibration. Ammonium acetate buffer (5 M, pH 4.7) was prepared by mixing 143 mL Optima grade acetic acid (17 M), 227.5 mL ammonium hydroxide (11 M) and 130 mL MQ water and subsequently purified by passing the solution through the Nobias extraction procedure (detailed below).

Estuarine and seawater samples with 'low' metal concentrations, and from which aliquots of 12–324 mL were required to provide sufficient Cd and/or Zn for isotope analysis, were preconcentrated using Nobias Chelate PA1 resin, using a procedure closely based on the method described in Conway et al., (2013) and slightly modified as described by Griffiths et al. (2020). Acidified samples were transferred to pre-weighed, pre-cleaned Nalgene LDPE bottles. 1 mL of 0.01 M H<sub>2</sub>O<sub>2</sub> was added per 1 L of sample, along with <sup>111</sup>Cd-<sup>113</sup>Cd and <sup>64</sup>Zn-<sup>67</sup>Zn double spikes to achieve ratios of spike-derived to natural Zn and Cd of S/N  $\approx 1.2$  (Arnold et al., 2010; Xue et al., 2012; Bridgestock et al., 2014; Murphy et al., 2016). The double spike equilibration time varied by element and sample from 24 hours to 2 weeks, with some samples requiring a longer equilibration period for accurate Cd isotope analyses based on the reproducibility of full procedural duplicates. The pH of the samples was then adjusted to  $4.8 \pm 0.2$  (Griffiths et al., 2020) by adding 2 mL ammonium acetate buffer per L and the appropriate volume of ammonium hydroxide. For samples of less than 100 mL, approximately 300  $\mu\text{L}$  of ammonium acetate buffer was added to afford better control of pH changes. Next, pre-cleaned Nobias resin was added to the samples and resin-sample mixtures were shaken on a shaker table for 2 hours. The resin was separated from the samples by pouring through a Teflon 'extraction rig' using a vacuum pump. The in-house extraction rig comprises an acrylic vacuum chamber and 47 mm PFA filter assembly (Savillelex) with acid-cleaned polycarbonate membrane (5  $\mu\text{m}$  pore size, Whatman Nuclepore). The resin was then rinsed with  $\sim 150$  mL MQ water to remove residual seawater salts. Trace metals were eluted from the resin into clean Teflon beakers via repeated additions of 3 M HNO<sub>3</sub> (approximately 4 x 5 mL). Finally, sample eluates were evaporated, refluxed with 180  $\mu\text{L}$  concentrated HNO<sub>3</sub> and 20  $\mu\text{L}$  concentrated H<sub>2</sub>O<sub>2</sub> for  $>2$  h, and evaporated once more. The efficacy of the Nobias resin extraction procedure for the separation of Zn and Cd from water samples was examined by analyses of three reference seawater samples from the GEOTRACES program (Boyle et al., 2012; Bryan et al., 2021).

River water samples (TR1, TR2, TR3, THdis) were vacuum filtered through Sartorius polyamide membrane filters (0.2  $\mu\text{m}$ , 47 mm). Sample TR1 was acidified to pH 2 by the addition of 6 M HCl whilst the remaining three river water samples had pH values of less than 2 on collection. These river water samples, alongside estuarine water samples with 'high' metal concentrations from which aliquots of  $<5$  mL were sufficient for Cd and/or Zn for isotope analysis, were spiked directly with <sup>111</sup>Cd-<sup>113</sup>Cd and <sup>64</sup>Zn-<sup>67</sup>Zn double spikes to achieve S/N ratios  $\approx 1.2$ , evaporated, redissolved in 6 M HCl and refluxed for  $>24$  hours.

## 2.4 Solid and particulate phase sample processing

The four sulfide-rich rock samples (CA, TH1, TH2, ST), were milled to a powder in the laboratories of the Environmental Mineralogy and Geochemistry Group at the University of Huelva. About 50–200 mg of each sample was refluxed with 2–8 mL 15.6 M HNO<sub>3</sub> at 120 °C for 6 days, ultrasonicated and evaporated. Subsequently, 3–8 mL 6 M HCl was added and evaporated, before dissolution in 6 mL 6 M HCl. Solutions were centrifuged (20 min, 2000 rpm) in Teflon centrifuge tubes.

Particulate samples collected on Sartorius polyamide membrane filters from the filtration of two 2019 estuarine samples, O12-19 and C7-19 (designated O12-19p and C7-19p), were selected for analysis. Filters were halved using ceramic scissors that were washed prior to and between use with ethanol and MQ water.

One filter half ('leachate') was submerged in 10 mL 1 M ammonium acetate (pH 7) and agitated for 1 hr (200 rpm,  $10^3$  rpm). Journal Pre-proofs  $10^3$ .

The solutions were subsequently evaporated to near dryness before repeated addition and refluxing with 2 mL concentrated  $\text{HNO}_3$ . Once a clear solution was achieved, the solutions were evaporated to dryness. The second filter half ('bulk digest') was fully digested by refluxing with 10 mL concentrated  $\text{HNO}_3$  at 120 °C for 1 h, followed by evaporation. The digestion residues were then oxidised with 5 mL concentrated  $\text{HNO}_3$  and 0.4 mL 30%  $\text{H}_2\text{O}_2$  and evaporated at 100 °C. All digest and leachate samples were refluxed overnight with 3–5 mL 6 M HCl.

For quality control, powdered aliquots of the USGS reference materials Nod-P1 (~20 mg) and BCR-2 (~50 mg) were subjected to similar leaching and bulk digestion procedures. Powders were leached in 10 mL 1 M ammonium acetate (pH 7) and agitated for 1 h (200 rpm). The suspensions were then centrifuged in Teflon centrifuge tubes (10 min, 2000 rpm) to separate the solid and supernatant. The supernatants were dried and refluxed in 3 mL 6 M HCl. Additional powder aliquots of BCR-2 were digested by refluxing in a 2:1 mixture of concentrated HF and  $\text{HNO}_3$ , followed by evaporation and refluxing with 6 M HCl. Powder aliquots of Nod-P1 were digested by refluxing with 3 mL 6 M HCl.

Aliquots of all solid phase leachate and digest solutions were spiked with appropriate volumes of Zn double spike to achieve S/N ratios  $\approx 1.2$  (Note: Cd concentrations in particulate samples were too low for analysis). After addition of the double spike, the samples were dried, dissolved in 6 M HCl and refluxed overnight at 120 °C.

## 2.5 Cd and Zn purification and isotope analysis

All samples were purified for isotopic analysis following previously published protocols, (Maréchal et al., 1999; Archer and Vance, 2004; Arnold et al., 2010; Xue et al., 2012; Conway et al., 2013; Little et al., 2014; Murphy et al., 2016). In detail, samples were dissolved in 7 M HCl + 0.05%  $\text{H}_2\text{O}_2$  and first processed using columns with macroporous Bio-Rad AG MP-1M resin (Archer and Vance, 2004). The Cd fractions from the first stage were further purified using a two-stage column chemistry that employed small columns with anion-exchange and Eichrom TRU resins, followed by heptane extraction to remove organic residues (Murphy et al., 2016). Some sample aliquots from which only Zn was separated utilised a single, smaller column, also with AG MP-1M resin (Bridgestock et al., 2014). The Zn fractions were evaporated, refluxed in  $\sim 300$   $\mu\text{L}$  concentrated  $\text{HNO}_3$  overnight, then dissolved in 1 mL 2% (v/v)  $\text{HNO}_3$  for analysis. The Cd fractions were evaporated, converted to nitrate form by refluxing with  $\sim 300$   $\mu\text{L}$  concentrated  $\text{HNO}_3$  overnight, evaporated, then dissolved in 1 mL 2% (v/v)  $\text{HNO}_3$  for analysis.

Cadmium isotope measurements were conducted on a Nu Plasma II MC-ICP-MS using a CETAC ASX-112FR autosampler and an Aridus II or DSN-100 desolvation system equipped with Micromist glass expansion nebulisers (nominal uptake rate 100  $\mu\text{L min}^{-1}$ ). Following optimisation, the sensitivity for Cd often reached  $\sim 500$  V ppm $^{-1}$ . Faraday cups fitted with  $10^{11}$   $\Omega$  resistors were employed to simultaneously measure the ion beam currents at mass numbers 111 ( $^{111}\text{Cd}^+$ ), 112 ( $^{112}\text{Cd}^+$ ,  $^{112}\text{Sn}^+$ ), 113 ( $^{113}\text{Cd}^+$ ,  $^{113}\text{In}^+$ ), 114 ( $^{114}\text{Cd}^+$ ,  $^{114}\text{Sn}^+$ ), 115 ( $^{115}\text{In}^+$ ,  $^{115}\text{Sn}^+$ ) and 117 ( $^{117}\text{Sn}^+$ ), with the latter two monitored for interference corrections. Data acquisition consisted of 60 x 5 s integration cycles after a 15 s baseline measurement during which the electrostatic analyser deflected the ion beam, and followed by a thorough wash sequence of 4 min (Ripperger et al., 2007).

The Cd isotope compositions of the samples, corrected for instrumental and any laboratory-induced mass bias, were calculated offline using an iterative double spike data reduction scheme, as outlined by Siebert et al. (2001). The results are reported using the  $\delta^{114}\text{Cd}$  notation:

$$\delta^{114}\text{Cd} = \left( \frac{{}^{114}\text{Cd}/{}^{110}\text{Cd}_{\text{sample}}}{{}^{114}\text{Cd}/{}^{110}\text{Cd}_{\text{NIST 3108}}} - 1 \right) \times 1000$$

whereby the  $\delta^{114}\text{Cd}$  values of samples are reported relative to the NIST 3108 Cd reference material. To this end, the samples were analysed interspersed between runs of a spiked NIST 3108 Cd solution, which had S/N ratios and total Cd concentrations that matched the samples to within  $\pm 10\%$  and  $\pm 25\%$ , respectively.

The analytical precision of multiple measurements of the spiked NIST 3108 Cd solutions within a measurement session was typically about  $\pm 0.06\%$  for  $\delta^{114}\text{Cd}$  (2 SD). Repeated analyses of the secondary



BAM-1012 Cd isotope standard yielded a  $\delta^{114}\text{Cd}$  value of  $-1.33 \pm 0.08\%$  ( $n = 61$ , 2 SD) in excellent agreement with [redacted] et al., (2020) and Murphy et al., (2016), respectively. The Cd concentrations of samples were determined using isotope dilution.

Zinc isotope measurements were carried out on a Nu Plasma HR MC-ICP-MS. Samples were introduced via a CETAC ASX-110 autosampler and an Aridus II or DSN-100 desolvation system used with Micromist glass expansion nebulisers (nominal uptake rate  $100 \mu\text{L min}^{-1}$ ). The MC-ICP-MS was operated in low-resolution mode and instrumental parameters were adjusted to maximise signal stability and sensitivity, whereby the latter was on average  $\sim 100 \text{ V ppm}^{-1}$  for Zn. For the analyses, the ion beams at mass numbers 62 ( $^{62}\text{Ni}^+$ ), 64 ( $^{64}\text{Zn}^+$ ,  $^{64}\text{Ni}^+$ ), 66 ( $^{66}\text{Zn}^+$ ), 67 ( $^{67}\text{Zn}^+$ ), 68 ( $^{68}\text{Zn}^+$ ), 68.5 ( $^{137}\text{Ba}^{2+}$ ) were collected simultaneously using Faraday cups equipped with  $10^{11} \Omega$  resistors. Each sample or standard run encompassed 3 blocks of  $20 \times 5 \text{ s}$  integration cycles and was preceded by a short analysis ( $20 \times 5 \text{ s}$  integrations) of 2%  $\text{HNO}_3$ . The latter measurement served to determine residual background signals for the isotopes of interest and these were subsequently subtracted from the sample and standard signals (Little et al., 2019). Each sample or standard measurement was followed by a 3 min wash sequence with 2%  $\text{HNO}_3$ .

As for Cd, the instrumental mass bias was corrected by the double spike technique, as outlined in (Arnold et al., 2010) and (Bridgestock et al., 2014), with the data reduction carried out offline following a procedure adapted from Siebert et al., (2001). Isobaric interferences from  $^{64}\text{Ni}$  and  $(^{136}, ^{134}, ^{132})\text{Ba}^{2+}$  were monitored during the analyses at mass numbers 62 and 68.5, respectively, and appropriate corrections were introduced during the offline data reduction. The interference levels determined for samples were almost negligible, with  $^{64}\text{Ni}/^{64}\text{Zn}$ ,  $^{132}\text{Ba}^{2+}/^{66}\text{Zn}$ ,  $^{134}\text{Ba}^{2+}/^{67}\text{Zn}$  and  $^{136}\text{Ba}^{2+}/^{68}\text{Zn}$  ratios of typically less than  $4 \times 10^{-5}$ .

The Zn isotope compositions of samples are reported using the common  $\delta^{66}\text{Zn}$  notation:

$$\delta^{66}\text{Zn} = \left( \frac{{}^{66}\text{Zn}/{}^{64}\text{Zn}_{\text{sample}}}{{}^{66}\text{Zn}/{}^{64}\text{Zn}_{\text{JMC-Lyon}}} - 1 \right) \times 1000$$

whereby  $\delta^{66}\text{Zn}$  was initially calculated relative to bracketing standard runs of the AA-ETH Zn isotope reference material. AA-ETH Zn solutions were mixed with the Zn double spike to yield total Zn concentrations and S/N ratios that matched the samples to within 10%. The final  $\delta^{66}\text{Zn}$  values are reported relative to the JMC Lyon Zn isotope reference material. To this end, the  $\delta^{66}\text{Zn}$  values originally measured relative to AA-ETH Zn were adjusted for an offset of  $+0.30\%$ , following the recommendations of Moynier et al., (2017) and Archer et al., (2017).

Multiple measurements of the spiked Zn standard solutions within a measurement session yielded analytical precisions of typically about  $\pm 0.05\%$  for  $\delta^{66}\text{Zn}$  (2 SD). The secondary in-house "London Zn" isotope standard was analysed during each measurement session and yielded a long-term average value of  $+0.10 \pm 0.05\%$  ( $n = 40$ , 2 SD) relative to JMC Lyon, in excellent agreement with previous results of  $+0.08 \pm 0.04\%$  ( $n = 10$ , 2 SD) and  $+0.12 \pm 0.04\%$  ( $n = 6$ , 2 SD) reported by Arnold et al. (2010) and Larner and Rehkämper (2012), respectively. Zinc concentrations of the samples were determined using isotope dilution.

## 2.6 Data quality control: Blanks and Reference Materials

Mean Cd blanks for the Nobias resin extraction and column chemistry were determined separately and were both low, at  $31 \pm 16 \text{ pg}$  ( $n = 11$ , 1 SD) and  $48 \pm 76 \text{ pg}$  ( $n = 21$ , 1 SD), respectively. Together, these blanks amount to less than 1% of the Cd present in the processed samples. The water filtration blank was evaluated by filtration of distilled water at the University of Huelva and subsequent analysis by QQQ-ICP-MS at the University of Montpellier (see Supplementary Text). The contribution of the filtration blank to the dissolved phase trace metal concentration data can only be calculated for Zn because Cd concentrations in the filtration blank were below the detection limit. The values for Zn are low for samples from the Odiel and Tinto branches of the estuary (with blank additions of between 0.01 and 0.5%) but increase in the samples from the common channel (up to 3.5%) and in the Gulf of Cadiz (up to 5.5%). We consider these filtration blanks to be maximum values, assuming a constant Zn blank mass that was diluted in a larger water volume for samples collected for isotope analysis. Hence, no filtration blank corrections were made. The mean Zn blank of the column chemistry was  $0.40 \pm 0.17 \text{ ng}$  ( $n = 20$ , 1 SD), which is negligible in comparison to the indigenous Zn of the samples, which was consistently  $>100 \text{ ng}$ . The blank for the Nobias resin extraction procedure was higher,

The Cd and Zn concentrations of Nobias-extracted samples determined by isotope dilution are blank corrected. The Cd blank contribution was low enough to have no significant impact on  $\delta^{114}\text{Cd}$  values of samples, so  $\delta^{114}\text{Cd}$  values are not blank corrected. For Zn, the Nobias resin extraction procedure was utilised for seven water samples (C5-19, C2-19, S38-19, S67-19, F30-19, G42-19, S67-17). Assuming a  $\delta^{66}\text{Zn}$  value of the Zn blank of between  $-0.1\text{‰}$  and  $+0.4\text{‰}$ , mass balance calculations can be carried out to assess its potential impact on  $\delta^{66}\text{Zn}$  values. For sample S67-17, containing  $2.5\ \mu\text{g}$  of Zn, a Zn blank of  $11\ \text{ng}$  contributes less than 0.5% to the total Zn budget of the sample, which is insignificant. For five samples (C5-19, C2-19, S38-19, S67-19, F30-19), the Zn blank accounts for between 4% and 10% of the total Zn present. For these samples, the Zn blank may alter the measured  $\delta^{66}\text{Zn}$  values by up to  $0.05\text{‰}$ , which is similar to or less than the analytical precision. For sample G42-19, the Zn blank contributes 18% to the total Zn budget. In this case, the blank could change the measured sample Zn isotope composition by up to  $0.11\text{‰}$ , approximately twice the analytical error. Accordingly, the Zn isotope composition of G42-19 is attributed a larger uncertainty.

Three seawater samples that were collected as part of the GEOTRACES programme, GDI, 1962 and 2268, were analysed as quality control materials in this study. The GEOTRACES deep intercalibration sample GDI was obtained from 2000 m depth at the BATS (Bermuda Atlantic Time Series) Station during the 2008 GEOTRACES Atlantic intercalibration cruise (Xue et al., 2012). Samples 1962 and 2268 were collected on the 2010 GEOTRACES GA10 cruise to the South Atlantic at stations 18 and 21, at depths of 3983 m and 2987 m, respectively. The three GEOTRACES samples were filtered and acidified to pH 2 shortly after collection following GEOTRACES protocols (Wyatt et al., 2014). The Cd and Zn concentrations and isotope compositions determined for the three GEOTRACES seawater samples yielded results that are identical, within uncertainty, to previously published values for the same or comparable samples (Table 1). No Zn isotope reference values are available for GDI. However, the GDI  $\delta^{66}\text{Zn}$  value reported here ( $+0.36 \pm 0.05\text{‰}$ ) agrees well with data obtained for seawater collected at the same depth at Station 10 of the GA03 transect ( $31.50\ \text{N}$ ,  $64.10\ \text{W}$ ), which is proximal to the BATS site from where GDI was collected ( $+0.38 \pm 0.03\text{‰}$ ; Conway and John, 2014).

Zinc isotope compositions obtained for bulk digested USGS reference materials agree with results from previous studies (Table 3; e.g., Chapman et al., 2006; Moeller et al., 2012; Moynier et al., 2017; Little et al., 2019; Pickard et al., 2022). The cellulose membrane filters used in 2017 were found to have high Zn contents, hence, particulate data for 2017 are not presented. Average digest and leachate Zn blanks of the Sartorius polyamide filters used in 2019 were  $36\ \text{ng}$  and  $78\ \text{ng}$ ,  $\sim 1\%$  and  $\sim 5\%$  of sample Zn contents, respectively. Reported particulate Zn concentrations (but not isotopic compositions) are blank corrected (Table 3).

Overall, the generally excellent agreement of the new and published trace metal concentration and isotope data validates the performance of the sample preparation procedures, including the Nobias extraction, double spiking, and mass spectrometry protocols.

### 3. Results

#### 3.1 Sulfide deposits and river water samples

The sulfide samples (ST, TH1, TH2, CA) have Cd concentrations of  $0.349\ \mu\text{g g}^{-1}$  to  $25.7\ \mu\text{g g}^{-1}$  and Zn concentrations of  $0.160\ \text{mg g}^{-1}$  to  $23.1\ \text{mg g}^{-1}$  (Table 2). Black shale hosted sulfide samples from Tharsis (TH1 and TH2) have Zn concentrations two orders of magnitude higher than the volcanic massive sulfides from Corta Atalaya (CA) and San Telmo (ST) mine sites. Tharsis mine samples are isotopically lighter for Zn (with  $\delta^{66}\text{Zn}$  of  $-0.01\text{‰}$  and  $+0.10\text{‰}$ ) compared to Corta Atalaya ( $+0.16\text{‰}$ ) and San Telmo ( $+0.29\text{‰}$ ) (Table 2, Figure 3). San Telmo also exhibits the most positive  $\delta^{114}\text{Cd}$  value, at  $+0.07\text{‰}$ . Samples from the other two mines have indistinguishable  $\delta^{114}\text{Cd}$  values of  $-0.10\text{‰}$  and  $-0.14\text{‰}$  (Figure 3).

Consistent with the high solid-phase Cd and Zn concentrations of the Tharsis sulfide samples, the river water sample collected proximal to the Tharsis mine in a tributary of the Odiel River (THdis) has the highest dissolved metal concentrations of  $24.8\ \mu\text{mol kg}^{-1}$  Cd and  $18.1\ \text{mmol kg}^{-1}$  Zn. Freshwater samples from close to the Corta Atalaya mine (TR1 and TR2), and downstream from these sites in the Tinto River (TR3), all have concentrations an order of magnitude lower than at Tharsis, but which increase downstream, with [Cd] from  $42.6\ \text{nmol kg}^{-1}$  to  $2990\ \text{nmol kg}^{-1}$  and [Zn] from  $172\ \mu\text{mol kg}^{-1}$  to  $1290\ \mu\text{mol kg}^{-1}$ . Sample TR1, chosen to represent 'natural background' sulfide weathering due to its location upstream of AMD-influenced tributaries,

has a Cd concentration an order of magnitude lower than TR2 (42.6 nmol kg<sup>-1</sup> vs 885 nmol kg<sup>-1</sup>). By contrast, TR1 and TR2 are isotopically indistinguishable for Zn (with  $\delta^{66}\text{Zn}$  of +0.35‰ and +0.34‰) but very different for Cd, with  $\delta^{114}\text{Cd}$  values of +0.48‰ and -0.13‰, respectively.

### 3.2 Ria of Huelva and Gulf of Cadiz samples

In 2017, the pH in the Odiel branch of the estuary ranged from 3.57 to 7.46 (O12-17, C5-17) and from 7.14 to 7.75 in the Gulf of Cadiz (S38-17, S67-17, F30-17, G42-17) (Table 2, Figure 4). In 2019, pH values increased from 5.09 to 8.82 (O15-19, C2-19) in the estuary and ranged from 8.08 to 8.16 in the Gulf of Cadiz.

Dissolved Cd and Zn concentrations in the Ria of Huelva estuary steadily decreased with increasing pH seawards (Figure 5). In 2019, dissolved Cd concentrations ranged from 128 nmol kg<sup>-1</sup> (O15-19) at the upper portion of the Odiel branch of the estuary to 0.588 nmol kg<sup>-1</sup> (C2-19) ~26.5 km downstream at the mouth of the estuary (Table 2, Figure 5A). Equivalent dissolved Zn concentrations ranged from 40.6  $\mu\text{mol kg}^{-1}$  to 0.089  $\mu\text{mol kg}^{-1}$  (Table 2, Figure 5B). In 2017, immediately following the La Zarza spill event, concentrations were 1.2 to four times higher than for the corresponding 2019 samples for Cd, and three to seven times higher for Zn. The most metal-rich sample is O12-17, with Cd and Zn concentrations of 228 nmol kg<sup>-1</sup> and 114  $\mu\text{mol kg}^{-1}$ , respectively. At the mouth of the estuary, Cd and Zn concentrations decreased to 0.717 nmol kg<sup>-1</sup> and 0.625  $\mu\text{mol kg}^{-1}$  respectively (C2-17). Two samples from the Tinto branch of the Ria of Huelva estuary were collected in 2019. At the upper end of the estuary, TR9 has dissolved Cd and Zn concentrations of 163 nmol kg<sup>-1</sup> and 55.5  $\mu\text{mol kg}^{-1}$ , respectively. Further downstream, TRX has 26.7 nmol kg<sup>-1</sup> Cd and 1.37  $\mu\text{mol kg}^{-1}$  Zn (Table 2). High metal and particularly Cd levels were determined for the process water (PW) of the phosphogypsum stacks, with Cd and Zn concentrations of 144  $\mu\text{mol kg}^{-1}$  and 1530  $\mu\text{mol kg}^{-1}$ , respectively.

The trace metals from the Ria of Huelva estuary form a plume of metal-enriched surface seawater in the Gulf of Cadiz. For Cd and Zn, the 2017 plume following the La Zarza spill had metal concentrations two to seven times higher than the plume in 2019. Average concentrations for the four 2017 Gulf of Cadiz samples (S38-17, S67-17, F30-17, G42-17) are  $0.601 \pm 0.24$  nmol kg<sup>-1</sup> (1 SD) for Cd and  $0.529 \pm 0.27$   $\mu\text{mol kg}^{-1}$  (1 SD) for Zn. In contrast, the four samples from the 2019 plume (S38-19, S67-19, F30-19, G42-19) have average Cd and Zn concentrations of  $0.313 \pm 0.044$  nmol kg<sup>-1</sup> (1 SD) and  $0.073 \pm 0.051$   $\mu\text{mol kg}^{-1}$  (1 SD), respectively.

The estuarine and seawater samples collected in 2017 and 2019 have nearly uniform dissolved Cd isotope compositions (Figure 6A). The average Cd isotope composition for the 2017 and the 2019 samples (from both the estuary and the Gulf of Cadiz) are  $+0.03 \pm 0.09$ ‰ (n = 10, 2 SD), and  $\pm 0.00 \pm 0.12$ ‰ (n = 9, 2 SD), respectively. All samples from both years, except O12-19 (-0.14‰), which appears to be an outlier, have Cd isotope compositions that are identical to one another within the analytical uncertainties.

In 2017, the  $\delta^{66}\text{Zn}$  values of the estuarine and Gulf of Cadiz samples ranged from +0.19‰ to -0.05‰, with a general decrease in  $\delta^{66}\text{Zn}$  towards, and into, the Gulf of Cadiz (Figure 6B). A similar pattern is observed in 2019, with an upper estuarine  $\delta^{66}\text{Zn}$  value of +0.20‰ (O15-19) and the lowest  $\delta^{66}\text{Zn}$  of -0.12‰ in the Gulf of Cadiz (G42-19). However, three samples in the Odiel branch of the estuary (O8-19, C7-19 and C5-19) lie off this trend, with more positive  $\delta^{66}\text{Zn}$  values of between +0.19‰ and +0.34‰ (circled: Figure 6B).

The two 2019 samples from the Tinto River branch of the Ria of Huelva estuary, TR9 and TRX, have Cd isotope compositions of +0.03‰ and +0.01‰ and Zn isotope compositions of +0.18‰ and +0.02‰, respectively. Process water (PW) from the adjacent phosphogypsum stack gave a  $\delta^{114}\text{Cd}$  value of -0.13‰ and a  $\delta^{66}\text{Zn}$  value of +0.35‰ (Table 2).

Table 3 displays Zn concentrations and isotope compositions for bulk digests and leachates of particulate samples collected at locations O12 and C7 in 2019 and for the USGS reference materials BCR-2 and Nod-P1. The mass of particulate Zn per volume of filtered water for the leached and digested portions of sample C7-19p are 23.0 and 66.2 nmol L<sup>-1</sup>, respectively. For O12-19p, the leached portion has 73 nmol L<sup>-1</sup> of Zn and the digested portion 149 nmol L<sup>-1</sup> of Zn. The  $\delta^{66}\text{Zn}$  values of the O12-19p digest and leachate are indistinguishable, at +0.58‰ and +0.60‰, respectively. Both are isotopically heavy compared to the dissolved Zn from this locality (+0.17‰). The C7-19p leachate is also isotopically heavier, at +0.51‰, than the corresponding C7-19 dissolved value, of +0.19‰, but the isotopic composition of the latter is identical to the C7-19 particulate digest. Leachate  $\delta^{66}\text{Zn}$  values for Nod-P1 (+0.81‰) and BCR-2 (+0.81‰) are either similar to (Nod P1: +0.79‰) or heavier than (BCR-2: +0.32‰) the respective bulk digests.

The following sections aim to decipher the relative influence of bedrock geology, riverine and/or estuarine biogeochemical processes, and additional anthropogenic sources to evaluate whether Cd and Zn isotope compositions can be used to trace AMD. A further intention is to better constrain the fluxes of dissolved Cd and Zn to the Gulf of Cadiz and beyond.

#### 4.1 Mine sulfide and freshwater AMD endmembers

The isotopic compositions of mine sulfide samples are within the range of previously measured  $\delta^{114}\text{Cd}$  and  $\delta^{66}\text{Zn}$  values for sulfide-rich rocks ( $-1.53\text{‰}$  to  $+0.34\text{‰}$  for Cd; e.g., Wombacher et al., 2003; Schmitt et al., 2009; Zhu et al., 2013;  $-0.17\text{‰}$  to  $+0.64\text{‰}$  for Zn; e.g., Mason et al., 2005; Wilkinson et al., 2005; Sonke et al., 2008; Fernandez and Borrok, 2009; Aranda et al., 2012; Skierszkan et al., 2016). With the exception of San Telmo, mine samples are isotopically light for Cd compared to the upper continental crust, estimated at  $+0.03 \pm 0.10\text{‰}$  by Pickard et al. (2022) with similar results by other workers (Schmitt et al., 2009; Rehkämper et al., 2011). For Zn, multiple analyses of ore-grade sphalerite yielded a  $\delta^{66}\text{Zn}$  of  $+0.16 \pm 0.2\text{‰}$  ( $n = 61$ , 2 SD) (Sonke et al., 2008). In general, as for Cd, the Zn isotope compositions of sulfides, including the samples analysed here, are lighter than igneous and clastic sedimentary rocks (at about  $+0.30 \pm 0.12\text{‰}$ ; Moynier et al., 2017) and average upper continental crust ( $+0.23 \pm 0.07\text{‰}$ ; Pickard et al., 2022). The preferential partitioning of isotopically light Cd and Zn into sulfides is consistent with theoretical *ab initio* calculations (Fujii et al., 2011; Yang et al., 2015), laboratory experiments (Archer, 2007; Guinoiseau et al., 2018b) and observations in natural settings (e.g. Schmitt et al., 2009; Vance et al., 2016; Xie et al., 2019; Bryan et al., 2021; Chen et al., 2021; Zhang et al., 2021).

Mine sulfide Cd and Zn isotope compositions show a positive correlation, with San Telmo isotopically heaviest and Tharsis isotopically lightest (Figure 7B). Although the limited sampling ( $n = 4$ ) precludes confident interpretation, and as a detailed discussion of ore deposit mineralisation is beyond the scope of this study, the co-variation in concentrations (Figure 7A) and isotopic compositions between mine sites may reflect the different pathways of sulfide mineralisation in volcano-sedimentary and volcanogenic settings (e.g., Wilkinson et al., 2005; John et al., 2008; Fujii et al., 2011; Zhu et al., 2013).

The freshwater samples THdis and TR2 both yield Cd isotope compositions within analytical error of sulfides from the proximal Tharsis and Corta Atalaya mines, respectively (Figure 3). Sample TR1 is distinct, with a low Cd concentration ( $42.6 \text{ nmol kg}^{-1}$ ) and a more positive  $\delta^{114}\text{Cd}$  value ( $+0.48\text{‰}$ ). Even though this value is a significant outlier from the remaining dataset (Figure 6A), other studies reported similar results for other AMD environments (e.g.,  $+0.64 \pm 0.03\text{‰}$  for AMD discharge in southern China; Yang et al., 2019). The unusually high  $\delta^{114}\text{Cd}$  value of TR1 is further supported by leaching experiments with a Pb-Zn ore, which yielded a leachate that was  $+0.50\text{‰}$  heavier than the original ore (Zhang et al., 2016). The lower Cd concentration of TR1 hence likely reflects 'natural background' sulfide weathering, which is the predominant source of metals in this stream, and releases less Cd compared to AMD. However, whether a process specific to natural sulfide weathering is the cause of the high  $\delta^{114}\text{Cd}$  value requires further investigations of sulfide mineral dissolution at varying degrees and rates of oxidation.

Alternatively, the combination of low [Cd] and high  $\delta^{114}\text{Cd}$  of TR1 may record preferential removal of isotopically light Cd via mineral or biological adsorption or uptake (Lacan et al., 2006; Horner et al., 2011; Wasylenki et al., 2014; Conway and John, 2015; Yan et al., 2021; Ratié et al., 2021; Wang et al., 2023). For example, experimental Cd adsorption onto Fe-(oxyhydr)oxides yielded  $\Delta^{114}\text{Cd}_{\text{solid-solution}}$  fractionations of approximately  $-0.5\text{‰}$  (Yan et al., 2021). Schwertmannite is an amorphous, orange-coloured Fe(III)-oxyhydroxysulfate mineral that forms in acidic environments at pH values of about 2.5 to 4.5 (Bigham et al., 1996; España et al., 2005b). Visual observations revealed orange precipitates in the stream at TR1 (pH = 2.6) but not at TR2 (pH = 1.5) (Figure 2), indicating the presence of schwertmannite at TR1. However, though schwertmannite is an important sink for Cd at neutral pH (Randall et al., 1999; Fan et al., 2019), it is predicted to have a positively charged surface at pH 2.6. Under these conditions, adsorption of  $\text{Cd}^{2+}$ , or even  $\text{CdSO}_4$ , would be unfavourable and should be negligible (Jönsson et al., 2005; Acero et al., 2006). Biological uptake and organic complexation of Cd appears to favour light isotopes (Lacan et al., 2006; Conway and John, 2015; Ratié et al., 2021). Only a limited number of organisms thrive at highly acidic conditions, including acidophilic bacteria, such as *Acidithiobacillus thiooxidans* and *Leptospirillum ferrooxidans* (Mielke et al., 2003), which catalyse the oxidative dissolution of sulfide minerals (Singer and Strumm, 1970). There is a paucity of research on acidophilic microorganisms and their metal uptake mechanisms (Costa et al., 2020), but the low

The freshwater samples TR1, TR2 and THdis show either the same or heavier Zn isotope compositions compared to proximal sulfide samples from the Corta Atalaya and Tharsis mines, respectively (Figure 3). Samples TR1 and TR2 have Zn concentrations of  $172 \mu\text{mol kg}^{-1}$  and  $535 \mu\text{mol kg}^{-1}$  and  $\delta^{66}\text{Zn}$  values of  $+0.35\text{‰}$  and  $+0.34\text{‰}$ , respectively. These samples are isotopically heavy compared to the Corta Atalaya volcanic-hosted sulfide sample at  $+0.16\text{‰}$ , resulting in a  $\Delta^{66}\text{Zn}_{\text{freshwater-sulfide}}$  of  $+0.18\text{‰}$ . Borrok et al. (2008) also measured water samples from close to the Corta Atalaya mine, from the Odiel River (Figure 3), and observed similar Zn concentrations and isotope compositions of about  $125 \mu\text{mol kg}^{-1}$  and  $+0.4\text{‰}$ . Sample THdis, from a tributary downstream of the Tharsis mine, has a  $\delta^{66}\text{Zn}$  of  $+0.08\text{‰}$ , effectively unfractionated relative to the Tharsis sulfide samples (TH1, TH2) at  $-0.01\text{‰}$  and  $+0.10\text{‰}$  (Figure 3).

In accord with these results, leaching studies of sphalerite and sulfide-rich rocks reported small variations in experimentally derived  $\Delta^{66}\text{Zn}_{\text{leachate-sulfide}}$  values, from  $\pm 0.0$  to  $+0.2\text{‰}$  (Fernandez and Borrok, 2009). Nevertheless, the leaching of sulfide-rich rocks from different regions has shown variable isotopic fractionations. Whilst several studies report leachates with  $\delta^{66}\text{Zn}$  values that are unfractionated relative to the rocks (Fernandez and Borrok, 2009; Skierszkan et al., 2016), some report lighter (Liu et al., 2020) or heavier (Fernandez and Borrok, 2009) leachate Zn isotope compositions. Observations from electron microprobe analyses suggest Zn can be associated with different mineral phases within sulfide-rich rocks, and this may explain the reported heterogeneity in  $\Delta^{66}\text{Zn}_{\text{leachate-sulfide}}$  (Fernandez and Borrok, 2009). Ultimately, the variable Zn isotope compositions of sulfide phases and of the Zn released from such minerals during weathering may be important drivers of the Zn isotope composition observed for rivers in the IPB.

Approximately 18 km downstream of the Tinto River headwaters (i.e., TR1 and TR2), the river at TR3 remains extremely acidic (pH 2.2) with much higher dissolved metal concentrations ( $[\text{Cd}] = 2990 \text{ nmol kg}^{-1}$ ,  $[\text{Zn}] = 1.29 \text{ mmol kg}^{-1}$ ), which reflect contributions from additional contaminated tributary streams (Nieto et al., 2013). The  $\delta^{114}\text{Cd}$  value at TR3 is  $+0.08\text{‰}$ , more similar to the strongly AMD-influenced stream sampled at TR2 than the isotopically heavy composition of TR1, consistent with much higher Cd concentrations for the AMD-influenced streams. The  $\delta^{66}\text{Zn}$  value of TR3 is less positive than both TR1 and TR2, at  $+0.16\text{‰}$  (Figure 3), suggesting the addition of isotopically light Zn from other AMD-influenced streams. This interpretation is supported by previous data for water samples collected in June 2006 from a similar location, which yielded a high average dissolved Zn concentration of  $2.06 \text{ mmol kg}^{-1}$  and an average  $\delta^{66}\text{Zn}$  value of about  $+0.25\text{‰}$  (Borrok et al., 2008).

At TR9, 63 km downstream in the Tinto branch of the Ria of Huelva estuary, the river has a higher pH (4.1), substantially lower Cd and Zn concentrations ( $163 \text{ nmol kg}^{-1}$  and  $55.5 \mu\text{mol kg}^{-1}$ , respectively) but essentially unchanged  $\delta^{114}\text{Cd}$  ( $+0.03\text{‰}$ ) and  $\delta^{66}\text{Zn}$  ( $+0.18\text{‰}$ ) values. These observations are best explained by a significant dilution of the waters between TR3 and TR9 by relatively uncontaminated streams and the intrusion of seawater. Unchanged  $\delta^{114}\text{Cd}$  and  $\delta^{66}\text{Zn}$  values imply that removal processes with associated isotope fractionation (e.g., mineral adsorption) are insignificant (Aranda et al., 2012; Matthies et al., 2014). Further, the pH in the river remains low, creating a proton-rich environment in which positive charges on particle surfaces electrostatically repel metal cations, thus reducing adsorption (Bonnissel-Gissing et al., 1998; Braungardt et al., 2003).

## 4.2 Estuarine Aqueous Chemistry

The ubiquitous AMD in the Huelva region is responsible for the very low pH values of approximately 2 for both the upstream Odiel and Tinto rivers. The pH increases by dilution with non-acidic waters and by mixing with seawater in the estuary. The extent of tidal intrusion and the position of the accompanying salinity front, where freshwater meets seawater, vary spatially and temporally due to a variety of factors, including tidal currents, wind, and river discharge (Gong and Shen, 2011; Molinas et al., 2014). Such variability is clearly observed in this study. In 2017, the pH in the Odiel branch of the estuary ranged from 3.57 to 7.46. The salinity front was much further inland in June 2019, due to the combination of low rainfall and a high tide, with a resulting pH range of 5.09 to 8.82 (Figure 4) and EC values akin to seawater ( $\sim 54 \text{ mS/cm}$ ) observed even in the upper reaches of the estuary, at O12-19 ( $55.1 \text{ mS/cm}$ , Figure S2). This variability is also reflected in the coastal Gulf of Cadiz surface water samples, which had a typical seawater pH of 8.1 in 2019 but were more acidic in 2017, at 7.14 to 7.75 (Figure 4). The larger freshwater influence in 2017 implies that a distinct salinity gradient was established in the Gulf of Cadiz at this time.

Figure 4). These values must be the result of processes other than binary mixing with seawater. Amaral et al. (2020) note that hypersalinity in the Huelva estuary is observed during periods of low freshwater flow and strong evaporation. Therefore, it is possible that the high salinity in 2019 increased the buffering capacity in the estuary via elevated concentrations of carbonate and bicarbonate ions (up to  $\text{pH} \approx 8.33$  was observed, but higher values are theoretically possible; de Souza Machado et al., 2016). Alternatively, or in addition, the elevated  $\text{pH}$  and chloride concentrations could be due to an alkaline effluent from the nearby industrial complex (see Section 4.3.3).

### 4.3 Biogeochemical cycling of Cd and Zn in Huelva estuary

#### 4.3.1 Conservative behaviour of Cd and Cd isotopes

The simplest model of an element's behaviour in an estuary assumes conservative mixing between riverine and seawater endmembers. Typically, conservative mixing is elucidated based on a linear relationship in  $[\text{Me}]$  (metal concentration) versus salinity. Here, in the absence of salinity measurements, chloride concentrations,  $[\text{chloride}]$ , are used as a proxy for seawater intrusion up-estuary. Focus is on the May 2017 dataset, due to the greater freshwater influence in 2017 that produces more variable chloride concentrations, and because of the unusually elevated chloride levels observed in parts of the estuary in 2019 (section 4.2). Measured  $[\text{Me}]$  versus  $[\text{chloride}]$  relationships for other sampling time points (throughout 2018 and in June 2019) are shown for reference in Figures S3 and S4.

A linear relationship is observed between  $[\text{chloride}]$  and  $[\text{Cd}]$  for the 2017 samples (Figure 8A) and, in large part, for other sampling time points throughout 2018 and 2019 (Figure S3). This relationship demonstrates generally conservative behaviour of Cd during mixing in the Ria of Huelva estuary. Conservative behaviour of Cd is consistent with studies in several other estuaries (Boyle et al., 1982; Edmond et al., 1985; Shiller and Boyle, 1991; Elbaz-Poulichet et al., 1996), and reflects chloride complexation of dissolved Cd above  $\text{pH}$  7 (Elbaz-Poulichet et al., 1987; Wasylenki et al., 2014). The formation of dissolved Cd-Cl complexes prevents particle scavenging and promotes desorption of Cd scavenged at lower salinities (Elbaz-Poulichet et al., 1987; Shiller and Boyle, 1991; Paalman et al., 1994; Dai and Martin, 1995).

The isotopic compositions of Cd in the upper portions of the estuary are comparable for the Odiel and Tinto branches in 2017 and 2019, as demonstrated by the  $\delta^{114}\text{Cd}$  values of  $-0.01\text{‰}$ ,  $+0.03\text{‰}$  and  $+0.04\text{‰}$  determined for O15-19, TR9 and O12-17, respectively. This upper estuarine  $\delta^{114}\text{Cd}$  value of about  $0\text{‰}$  is in accord with the Cd isotope compositions of the lower estuary and the proximal Gulf of Cadiz in both years, with an average of  $+0.01 \pm 0.10\text{‰}$  (all data,  $n = 21$ ). Overall, both  $[\text{Cd}]$  and  $\delta^{114}\text{Cd}$  are consistent with conservative behaviour of Cd in this environment (Figure 6A).

#### 4.3.2 Evidence for non-conservative behaviour of Zn and Zn isotopes

Previous studies indicate that the behaviour of Zn in estuaries is more complex than that of Cd, often involving non-conservative attenuation processes (Wang and Liu, 2003; Petit et al., 2015; Wang et al., 2017; Guinoiseau et al., 2018a). Zinc behaves non-conservatively in the Ria of Huelva estuary, as illustrated by the non-linear (concave) relationship of  $[\text{Zn}]$  with  $[\text{chloride}]$ , which indicates Zn removal to the particulate phase (Figure 8B; Figure S4).

The extent of Zn removal can be estimated by comparison of measured and modelled Zn concentrations that assume conservative mixing between seawater and a river water endmember. The seawater endmember is attributed the average  $[\text{chloride}]$  and  $[\text{Zn}]$  characteristics of contemporaneous Gulf of Cadiz samples, whilst the riverine endmember is assigned a chloride concentration of  $0\%$  (Table 2; Table S1, S2). The riverine Zn concentration is derived by mass balance from the composition of the most Zn-rich sample (in May 2017, O12-17), assuming conservative mixing upstream of this location. Based on its chloride concentration of  $0.95\%$ , O12-17 has a seawater fraction of  $0.47$ , yielding a hypothetical riverine  $[\text{Zn}]$  endmember of  $215 \mu\text{mol kg}^{-1}$  (Table S1, S2).

Figure 8C shows the observed and modelled Zn concentrations versus  $\text{pH}$ , and the calculated extent of Zn removal, of  $62\%$ , by comparison to the conservative mixing model. This simple model assumes no Zn removal (or addition; cf. Achterberg et al., 2003) upstream of location O12, and does not account for the addition of Zn at the confluence from the Tinto branch of the estuary. The modelled extent of removal is also sensitive to the chloride concentration attributed to the seawater endmember. Two samples (C5-17 and C2-

17) have chloride concentrations higher than the averaged Gulf of Cadiz samples (Model A, Table S2) and the

concentration is chosen to represent the seawater endmember rather than the Gulf of Cadiz average (S67-17, which also has lowest [Zn]), calculated Zn removal increases to 75% at pH 6.6 and to about 90% at pH 7.5 (Model B, Table S2). Similar patterns and extents of Zn removal are observed at different sampling time periods throughout 2018 (Figure S4 and S5), with maximum calculated extents of Zn removal ranging from 49 to 97%. The inferred estuarine Zn removal is similar to a previous estimate of 64% based on data from 1996 to 1998, which was calculated by comparison of the estimated combined Tinto and Odiel River Zn fluxes with an estimate of the Zn flux at the estuary/sea boundary (Braungardt et al., 2003).

The model-data comparison suggests that significant Zn scavenging occurs even at relatively low pH, with 35% Zn removal estimated for pH 5.5, increasing to at least 62% Zn removal at pH 6.6 (Figure 8C). Scavenging is likely to be associated with schwertmannite (pH  $\approx$  2–4), basaluminite (or other Al-mineral phases, pH  $\approx$  4–5) and ferrihydrite/goethite (pH  $\approx$  5–7), together believed to predominate under AMD conditions (España et al., 2005b; España et al., 2005a; España et al., 2006; Cánovas et al., 2007). An increase in scavenging intensity at pH 6 and above is consistent with prior studies (e.g., Skierszkan et al., 2016; Szykiewicz and Borrok, 2016). For example, experiments have demonstrated that the rate of Zn adsorption onto goethite increases at pH 6.5 irrespective of salinity (Balistrieri and Murray, 1982). These findings suggest that pH is a controlling variable for the removal of Zn from the dissolved phase (Braungardt et al., 2003; Nordstrom, 2011; Hierro et al., 2014).

Zinc isotope compositions in the upper reaches of the Odiel and Tinto branches of the estuary are similar for the two rivers and between years, at +0.15‰ to +0.20‰ (Figures 3 and 7), pointing to a consistent value of about +0.17‰ for AMD in the Huelva region. The  $\delta^{66}\text{Zn}$  values generally decrease above about pH 6 for the 2017 and 2019 estuarine samples, despite the different geographical locations of this pH change across the two years of sampling (Figure 6B). A similar pattern was observed in the Rio Grande watershed, USA, a basin influenced by natural acid rock drainage (Szykiewicz and Borrok, 2016). In the latter study, the more negative  $\delta^{66}\text{Zn}$  values observed for water samples above pH 7 were attributed to Zn adsorption onto particle surfaces (Skierszkan et al., 2016; Szykiewicz and Borrok, 2016).

Although this study does not present particulate Zn isotope data for samples collected in 2017, the  $\delta^{66}\text{Zn}$  values determined for the leachate (i.e., exchangeable) phase of particulate samples obtained at O12 and C7 in 2019 are +0.58‰ and +0.51‰ (Table 3). In the Ria of Huelva estuary, this exchangeable Zn is likely weakly adsorbed to Al- and Fe-oxides, which dominate particulate material in the estuary at about pH 7 (pH at O12 = 6.8 in 2019) (España et al., 2005a; España et al., 2005b; Cánovas et al., 2007). Iron and Al oxide phases preferentially adsorb isotopically heavy Zn (e.g., Pokrovsky et al., 2005; Balistrieri et al., 2008), consistent with the observed leachate isotopic compositions of O12-19p, C7-19p, and Nod P1. Compared to the associated dissolved phase data (Table 2), these results yield  $\Delta^{66}\text{Zn}_{\text{adsorbed-solution}}$  values of about +0.4‰, in accord with preferential adsorption of isotopically heavy Zn onto particulates.

A comparison of dissolved and total particulate Zn concentrations in 2019 indicates that the proportion of particulate Zn increases from 0.7% to 14% between O12 and C7 as the pH increases from 6.8 to 8.7. Modelling 10% to 15% Zn removal via either a Rayleigh or steady state approach, given an initial  $\delta^{66}\text{Zn}$  value of about +0.2‰ and  $\Delta^{66}\text{Zn}_{\text{adsorbed-solution}} = +0.4‰$ , yields a dissolved Zn isotope composition of about +0.1‰, within the range of those observed for the Huelva dataset in 2019 (Figure S6). However, the mixing model of Figure 8C indicates that up to about 62% of Zn was removed by adsorption in the Ria of Huelva estuary in 2017. For 62% Zn removal, both the Rayleigh and steady state models predict significantly lower dissolved  $\delta^{66}\text{Zn}$  values, of about  $-0.3‰$  and  $-0.1‰$  respectively, than are observed in this study (Figure 6B and S6). This finding indicates that total particulate Zn removal in 2017 was apparently associated with less isotope fractionation than implied by the  $\delta^{66}\text{Zn}$  values of the 2019 leachates.

One possible explanation for the absence of very light dissolved Zn isotope compositions is the removal of dissolved Zn to an additional, isotopically light, particulate Zn pool. This hypothesis is supported by the bulk digest results for C7-19p. The C7-19p digest has a  $\delta^{66}\text{Zn}$  of +0.19‰, isotopically lighter than the C7-19p leachate, at +0.51‰ (Table 3). By mass balance, the more “refractory” (i.e., non-exchangeable) Zn pool of C7-19p must therefore be even lighter, at  $\delta^{66}\text{Zn} \approx +0.02‰$ . The source of this light Zn could be organic, as cellular uptake typically involves preferential uptake of light Zn isotopes (e.g., John et al., 2007; Köbberich and Vance, 2017; 2019). Alternatively, a low particulate  $\delta^{66}\text{Zn}$  value may reflect co-precipitation of isotopically light Zn in Fe or Al oxide phases (Little et al., 2019), and/or kinetic isotope fractionation during precipitation of these phases associated with a strong turbidity gradient, as suggested for the Gironde Estuary (Petit et al., 2015). Hence, removal of isotopically light Zn in the mixing zone may partially compensate for the loss of

isotopically heavy Zn to adsorption elsewhere. Further microanalytical analyses targeted particulate phase samplings, and the isotopically light Zn pool, and how it may be related to the seasonal and/or annual changes in particulate fluxes within estuaries.

Finally, contrary to the generally decreasing dissolved  $\delta^{66}\text{Zn}$  values observed with increasing pH for the estuary in 2017, three samples from 2019 (O8-19, C7-19, C5-19; Figure 6B) show more positive  $\delta^{66}\text{Zn}$  values at high pH values (>8.1) and high chloride concentrations. These samples do not correspond to the high turbidity zone (as indicated by high pH and EC values; Figure S2), and the high  $\delta^{66}\text{Zn}$  values are hence unlikely to be a consequence of a precipitation-driven kinetic isotope effect. Isotopic fractionation due to biological uptake that is observed only in the confluence of the estuary, where Zn concentrations are relatively high, but not elsewhere, also appears unlikely. One possible explanation for these isotopically heavy dissolved signatures is an external anthropogenic source of Zn, which is discussed below.

### 4.3.3 Isotopic evidence for an industrial influence on $\delta^{66}\text{Zn}$

In 1988, the Andalusian Environmental Agency imposed a Remediation Plan to control the industrial effluents that enter the Ria of Huelva estuary (Sainz et al., 2004; Pérez-López et al., 2011). Nevertheless, and with the city of Huelva situated between the two tributaries of the Tinto and Odiel rivers, anthropogenic runoff (including sewage) and atmospheric deposition from urban and industrial activities still impact the estuary (Querol et al., 2002; Sánchez de la Campa et al., 2018). In particular, large industries, including a copper metallurgical complex as well as biomass power generation and petrochemical plants, are situated south of Huelva city, adjacent to the confluence of the estuary (Figure 1; Martín et al., 2002; Querol et al., 2002; Barba-Brioso et al., 2010; Pérez-López et al., 2011).

Anthropogenic sources of Zn have wide-ranging  $\delta^{66}\text{Zn}$  values. Combustion sources, in general, produce isotopically light aerosols ( $\delta^{66}\text{Zn} \approx -0.73\text{‰}$  to  $+0.21\text{‰}$ ; reviewed by Schleicher *et al.*, (2020) and references therein). In contrast, slag waste and tailings from pyrometallurgical processes are typically enriched in heavy Zn isotopes. For example, the tailings of a Zn smelter featured a mean  $\delta^{66}\text{Zn}$  of  $+0.74 \pm 0.43\text{‰}$  ( $n = 6$ , 2SD) (Sivry et al., 2008) and such products can enter nearby waterways (Sonke et al., 2008; Gelly et al., 2019; Desaulty and Petelet-Giraud, 2020). Aside from metal processing, there are multiple sources of Zn emissions in urban areas (Cloquet et al., 2006; Gonzalez et al., 2016; Dong et al., 2017; Souto-Oliveira et al., 2018). The wastewaters that enter the Ria of Huelva estuary from the industrial complexes were estimated to carry a Zn load of  $3393 \text{ kg y}^{-1}$  between 2003 and 2006, whereby pigment plants were considered to be the largest source of Zn pollution (Pérez-López et al., 2011). In comparison to the Zn discharged via AMD, these industrial inputs are insignificant, at approximately 0.1%. Nonetheless, the industrial wastewaters enter the estuary at its confluence, where the originally high Zn concentration from AMD has already fallen by more than a factor of 100 due to estuarine attenuation processes and seawater dilution. Estuarine sediments collected adjacent to the industrial complex were more enriched in Zn ( $279 \text{ mg kg}^{-1}$ ) than those from the mouth of the estuary ( $166 \text{ mg kg}^{-1}$ ), suggesting a possible industrial contribution to the particulate Zn budget (Torre et al., 2019).

As discussed in section 4.3.2, several estuarine samples from 2019 have unexpectedly heavy Zn isotope compositions, linked to elevated pH values and chloride concentrations. Specifically, these samples are O8-19 ( $\delta^{66}\text{Zn} = +0.34\text{‰}$ ), collected near to the city of Huelva, as well as C7-19 ( $\delta^{66}\text{Zn} = +0.19\text{‰}$ ) and C5-19 ( $\delta^{66}\text{Zn} = +0.22\text{‰}$ ), from locations proximal to the industrial complex. It is plausible that alkaline industrial effluents may be responsible for the abnormally high pH values and high chloride concentrations observed in the estuary confluence in 2019 (Figure 4). Four of 34 wastewaters from industrial plants in Huelva that were analysed in a previous investigation had pH values exceeding 8.5 (Pérez-López et al., 2011). Without further constraints on the Zn isotope compositions of possible industrial effluents, it cannot be ascertained with confidence whether such emissions contributed significantly to the Zn budget of the estuary. Nevertheless, it is possible that the high  $\delta^{66}\text{Zn}$  values of O8-19, C7-19 and C5-19 are due to an industrial source. Such a source is not apparent in the 2017 samples, either due to much higher AMD-derived Zn concentrations compared to 2019 or because industrial Zn emissions are temporally variable.

### 4.3.4 Phosphogypsum stack: a source of Cd?

Cadmium is often emitted from urban environments and industrial activities (Nriagu and Pacyna, 1988; Pacyna and Pacyna, 2001). The isotope fractionation induced by such processes can be very large, up to about 1‰ (Shiel et al., 2010), and Cd isotope ratios can hence be an effective tracer of industrial pollution (Gao et al., 2013; Zhong et al., 2021). High-temperature industrial processing generally appears to produce



isotopically light dust emissions ( $\delta^{114}\text{Cd} = -0.74 \pm 0.13\text{‰}$ , 2 SD) (Cloquet et al., 2006) and isotopically heavier resi

ong et al., 2021). A previous study estimated that approximately 33 kg y<sup>-1</sup> of Cd is discharged into the Ria of Huelva estuary (Pérez-López et al., 2011). However, estuarine Cd isotope compositions determined in this study do not vary significantly near sources of possible Cd emissions, suggesting that anthropogenic pollutants are not a significant source of Cd compared to AMD, except for the phosphogypsum stacks.

About 100 Mt of phosphogypsum waste from phosphoric acid production is stored in the tidal prism of the Ria of Huelva estuary (Pérez-López et al., 2007; Rentería-Villalobos et al., 2010; Pérez-López et al., 2010). Cadmium is highly enriched in both the phosphate rock precursor (about 1 to 11 mg kg<sup>-1</sup>; Pérez-López et al., 2007; Rentería-Villalobos et al., 2010) and the phosphogypsum waste (2 to 15 mg kg<sup>-1</sup>; Pérez-López et al., 2007; Rentería-Villalobos et al., 2010; Pérez-López et al., 2010) compared to upper continental crust (UCC, about 0.1 mg kg<sup>-1</sup>; Rudnick and Gao, 2003). Whilst Zn is also somewhat enriched in phosphate rock (about 200 mg kg<sup>-1</sup>, compared to 67 mg kg<sup>-1</sup> in UCC; Rudnick and Gao, 2003) it is depleted in the phosphogypsum waste (about 5 to 8 mg kg<sup>-1</sup>) (Rentería-Villalobos et al., 2010; Pérez-López et al., 2010). Process water is present around the base of the phosphogypsum waste stacks and large volumes rest on top of the stacks, exposed to the atmosphere to evaporate, which results in highly trace metal-rich, acidic solutions (Pérez-López et al., 2016; Guerrero et al., 2021).

Sample TRX, collected directly adjacent to the phosphogypsum stacks, is used to assess whether potential discharge from the stacks to the estuary can be traced, by comparison to sample TR9 from further upstream (Figure 9). The Zn and Cd concentrations of a process water (PW) sample are 1.53 mmol kg<sup>-1</sup> and 144 µmol kg<sup>-1</sup>, respectively, akin to concentrations of 4.36 mmol kg<sup>-1</sup> for Zn and 449 µmol kg<sup>-1</sup> for Cd measured by Papislioti et al., (2018). The Cd/Zn ratio of the process water (ca. 0.1) is thus two orders of magnitude higher than that typical of AMD (ca. 0.002). Although dilution decreases the absolute Cd and Zn concentrations of TRX compared to TR9, the Cd/Zn ratio increases markedly from 0.003 at TR9 (comparable to Cd/Zn ratios for the Odiel branch of the estuary) to 0.02 at TRX and it remains elevated at C7-19 and C5-19 (~0.01).

Consistent with the elevated dissolved Cd/Zn ratios observed in this study, Pérez-López et al., (2016) calculated that the phosphogypsum stacks release 1.6 ton y<sup>-1</sup> of Cd, equivalent to ~15% of the annual average Cd discharge of 11 ton y<sup>-1</sup> from the Tinto and Odiel Rivers (Olías et al., 2006). By comparison, the equivalent phosphogypsum Zn contribution is approximately 0.3%. Mass balance can be used to calculate the impact of phosphogypsum discharge on the riverine Cd isotope composition at TRX, assuming a 15% Cd phosphogypsum contribution (as proposed by Pérez-López et al., 2016) with a  $\delta^{114}\text{Cd}$  of  $-0.13\text{‰}$ , as defined by the process water sample (Table 2, Figure 8C). Mixing with TR9, at  $+0.03\text{‰}$ , suggests a  $\delta^{114}\text{Cd}$  of  $+0.01\text{‰}$  at TRX, consistent with the measured value (Table 2; Figure 9). Hence, though industrial and urban Cd sources elsewhere in the Huelva region appear negligible, a significant emission of Cd from the phosphogypsum stacks to the estuary is consistent with the Cd isotope data and the elevated Cd/Zn ratios. At present, it is unclear whether process water or lateral edge outflows of contaminated water are responsible for the contamination of the estuary by phosphogypsum stack emissions (Pérez-López et al., 2015; Pérez-López et al., 2016; Papislioti et al., 2018; Guerrero et al., 2019).

#### 4.4 Tracing acid mine drainage: evidence from the 2017 La Zarza mine spill

On 17 May 2017 there was a spill at the abandoned La Zarza mine (Olías et al., 2019). The spill was caused by an increasing volume of stored water in the open pit, which finally exerted too much pressure on a concrete plug in the Los Cepos gallery of the mine. Consequently, ~270,000 m<sup>3</sup> of extremely polluted AMD was released into the local water systems (Olías et al., 2019). Before the spill and after the concrete plug was installed in the 1990s there was a moderate flux of acidic water from the Los Cepos gallery, with Cd and Zn concentrations of 0.116–0.178 µmol kg<sup>-1</sup> and 61.2–122 µmol kg<sup>-1</sup>, respectively (España et al., 2005a; Olías et al., 2019). Following the spill, the Cd and Zn concentrations of the released water increased to 3.91 µmol kg<sup>-1</sup> and 2126 µmol kg<sup>-1</sup>, respectively. The maximum concentrations peaked two weeks after the discharge, on 31 May, and the effects were observed for a month afterwards (Olías et al., 2019).

The data presented in this study demonstrate marked differences in dissolved Cd and Zn concentrations for estuarine waters collected in 2017, 2018 and 2019 (Figure 5; Figure S3 and S4). Yet, even though the 2017 metal concentrations exceed the 2019 values by more than a factor of x2, this does not translate into variable Cd and Zn isotope compositions. The mean  $\delta^{114}\text{Cd}$  values are  $+0.03 \pm 0.09\text{‰}$  (n = 10, 2 SD) and  $\pm 0.00 \pm 0.12\text{‰}$  (n = 9, 2 SD) for 2017 and 2019, respectively. The equivalent mean  $\delta^{66}\text{Zn}$  values for the estuarine

and Gulf of Cadiz samples are  $+0.08 \pm 0.14\%$  ( $n = 10$ , 2 SD) for 2017 and  $+0.11 \pm 0.27\%$  ( $n = 11$ , 2 SD) for 2019.

the Odiel and Tinto Rivers in 2019, despite large variations in riverine metal concentrations. Taken together, these findings suggest that Cd or Zn isotope compositions are unlikely to be useful tracers for linking the origin of AMD to specific mines or mining districts. Nevertheless, on a broader scale, the homogenous AMD signature is distinct from non-AMD influenced rivers, which are characterised by  $\delta^{114}\text{Cd}$  and  $\delta^{66}\text{Zn}$  values of about  $+0.2\%$  and  $+0.3\%$ , respectively (e.g., Chen et al., 2008; Lambelet et al., 2013; Little et al., 2014). Further work should investigate the extent to which the isotopically light AMD signature from the IPB can be traced, both spatially (see section 4.5) and temporally (e.g., via sediment core analyses).

#### 4.5 Broader impacts of AMD on the Gulf of Cadiz and beyond

It has been estimated that the Tinto and Odiel Rivers supply approximately 0.37% and 15% of the total global riverine dissolved flux of Cd and Zn, respectively (Sarmiento et al., 2009). However, the potential attenuation of the trace metal fluxes in the Ria of Huelva estuary was not considered in these estimates. Whilst the results of this study indicate that Cd displays conservative behaviour in the estuary, mixing calculations suggest that as much as 62% of Zn was removed to the particulate phase in the estuary in 2017. Non-conservative behaviour of Zn is also observed for other sampling time periods during 2018 (removal of 49 – 97%), though is more difficult to ascertain for June 2019, due to the low freshwater flow and extensive tidal intrusion up the estuary during sampling (Figure S4). Evidence from the particulate load indicates that at least 14% of total Zn was removed to the particulate phase in 2019. Both dissolved and particulate metal fluxes reveal significant temporal variations (e.g., 11–9040  $\mu\text{mol kg}^{-1}$  [Zn] in the Tinto River; Olías et al., 2006) rendering flux estimates difficult. Nevertheless, the non-conservative behaviour of Zn suggests that the dissolved Zn flux into the Gulf of Cadiz has been over-estimated.

Despite marked estuarine removal of dissolved Zn, both Cd and Zn concentrations in Gulf of Cadiz surface waters are typically about two orders of magnitude higher than observed in surface waters of eastern North Atlantic (Conway and John, 2014; Conway and John, 2015). In 2019, Gulf of Cadiz surface waters near the mouth of the Ria of Huelva estuary exhibited mean Cd and Zn concentrations of  $0.313 \pm 0.044$   $\text{nmol kg}^{-1}$  (1SD) and  $0.073 \pm 0.051$   $\mu\text{mol kg}^{-1}$  (1SD), respectively. These concentrations are consistent with prior results from between 1996 and 1999, of approximately 0.9  $\text{nmol kg}^{-1}$  for Cd and 0.1  $\mu\text{mol kg}^{-1}$  for Zn (Elbaz-Poulichet et al., 2001). The concentrations are seasonally very variable (Elbaz-Poulichet et al., 2001) and catastrophic events such as the La Zarza spill in 2017 contribute to the unpredictability of trace metal fluxes to the Gulf. Notably, Gulf of Cadiz surface waters had higher metal concentrations in 2017 compared to 2019, with results of  $0.601 \pm 0.24$   $\text{nmol kg}^{-1}$  (1SD) and of  $0.529 \pm 0.27$   $\mu\text{mol kg}^{-1}$  (1SD) for Cd and Zn, respectively.

To date, the only Cd and Zn isotope data available for the open ocean proximal to the Gulf of Cadiz region are for sampling stations of the GEOTRACES GA03 cruise, which sailed from Lisbon, Portugal into the North Atlantic Ocean in 2010 (Conway and John, 2014). The Cd isotope compositions of samples collected from the Gulf of Cadiz in 2017 and 2019 are narrow in range, from  $+0.01\%$  to  $+0.05\%$  ( $n = 6$ ), compared to  $\delta^{114}\text{Cd}$  values that exceed  $+0.5\%$  in the eastern North Atlantic (Conway and John, 2015). Zinc isotope compositions in the Gulf of Cadiz range from  $-0.12\%$  to  $+0.12\%$ , within the range of typical open ocean surface  $\delta^{66}\text{Zn}$  values, though these vary widely. For example, values of  $+0.40\%$  to  $-0.27\%$  were observed in the upper 50 m of the water column at Station 1 of the GA03 GEOTRACES cruise (Conway and John, 2014).

Circulation inshore on the Gulf of Cadiz continental shelf is comprised of two alternating currents, an eastward current and a coastal countercurrent, which circulate around the coastline from Cape Santa Maria to the Guadalquivir River, passing the mouth of the Ria of Huelva estuary (Figure 10; Peliz et al., 2009; Garel et al., 2016; Laiz et al., 2020). Laiz et al., (2020) estimate that westward flow from the coastal Gulf of Cadiz is present approximately 40% of the time, resulting in a significant potential flux of trace metals from the Iberian Pyrite Belt to the Atlantic Ocean. Offshore, the circulation in the Gulf of Cadiz upper slope region also consists of two opposing currents (Figure 10; Peliz et al., 2009). Spanish Shelf Water (SSW), also known as the Gulf of Cadiz Current (Peliz et al., 2009), flows eastward at shallow depths towards the Strait of Gibraltar, while Mediterranean Outflow Water (MOW), distinguished by its high salinity, flows westward at depths of approximately 400 m towards the Atlantic (Peliz et al., 2009; Mulero-Martínez et al., 2021). It is widely accepted that trace metal-rich waters from the Ria of Huelva estuary, with additional fluxes from the Guadalquivir and Piedras Rivers, are transported east along the coast through the Strait of Gibraltar by SSW (Elbaz-Poulichet et al., 2001). The inflow of SSW through the Strait of Gibraltar is the main source of trace metals to the western Mediterranean basin (Van Geen et al., 1988; van Geen and Boyle, 1990; Van Geen et al., 1991; Elbaz-Poulichet et al., 2001; Laiz et al., 2020).

Sampling campaigns with improved spatial and temporal coverage will be necessary to better constrain the fate and transport of AMD. The results of this study already suggest, however, that isotopic analysis may prove a useful tool in this endeavour, given the Cd and Zn enrichment and isotopically light AMD signature of Cd and Zn sourced from the Huelva region.

## 5. Conclusion

The results of this study show that the distinct  $\delta^{114}\text{Cd}$  and  $\delta^{66}\text{Zn}$  signatures of local mining districts in the IPB are not reflected in variable isotopic compositions of the ensuing AMD. Instead, the Odiel and Tinto rivers present accumulated and uniform  $\delta^{114}\text{Cd}$  and  $\delta^{66}\text{Zn}$  values of about +0.02‰ and +0.17‰, respectively, which render isotopic tracing of specific mines or mining districts in the Iberian Pyrite Belt using Cd and Zn difficult.

The AMD-sourced  $\delta^{114}\text{Cd}$  value of the rivers does not vary within the Ria of Huelva estuary, in accord with the generally observed conservative estuarine behaviour of the element. The elevated Cd/Zn ratios determined for some water samples reflect addition of Cd to the Tinto branch of the Ria of Huelva estuary from adjacent phosphogypsum stacks. For Zn, samples collected between 2017 and 2019 indicate non-conservative behaviour in the estuary, with removal of 49 to 97% of dissolved Zn to the particulate phase. Dissolved  $\delta^{66}\text{Zn}$  values decrease following the onset of adsorption, but not to the extent predicted by a fractionation factor of  $\Delta^{66}\text{Zn}_{\text{adsorbed-solution}} \approx +0.4\text{‰}$  for adsorption to particles, as inferred from isotopic analyses of estuarine particulates. The absence of the expected low dissolved  $\delta^{66}\text{Zn}$  values suggests a possible missing sink for isotopically light Zn within the estuary. In 2019, unusually high pH values (pH = 8.8) and chloride concentrations (2.74%) in the estuary coincide with more positive dissolved estuarine  $\delta^{66}\text{Zn}$  values, potentially due to anthropogenic inputs from nearby industrial activities.

The La Zarza mine spill event in 2017 had no significant impact on the dissolved Cd and Zn isotope compositions in the Ria of Huelva estuary. However, regionally, the estuarine waters entering the Gulf of Cadiz have high, if variable, Cd and Zn concentrations coupled with distinct and relatively constant light isotope compositions. The influence of the AMD plume may reach the Atlantic and Mediterranean Oceans, highlighting that Cd and Zn isotopes may be useful tracers for the regionally averaged AMD inputs originating from the Iberian Pyrite Belt.

## 6. Acknowledgements

The authors would like to thank Simon Hohl and two anonymous reviewers for helpful comments that improved the manuscript. H.P. was supported by the Natural Environment Research Council DTP “Science and Solutions for a Changing Planet” (NE/L002515/1) at Imperial College London. S.H.L is supported by a NERC Independent Research Fellowship (NE/P018181/2). The research was also funded by the Spanish Ministry of Economy and Competitiveness under research project TRAMPA (MINECO; PID2020-119196RB-C21). M.D.B. thanks the Spanish Ministry of Science and Innovation for the Postdoctoral Fellowship granted under application reference IJC2018-035056-I.

## Appendix A: Supplementary Material

Supplementary material contains Supplementary Text (Methods), Supplementary Table S1 and Supplementary Figures S1 – S6.

## References

- Acerro P., Ayora C., Torrentó C. and Nieto J. M. (2006) The behavior of trace elements during schwertmannite precipitation and subsequent transformation into goethite and jarosite. *Geochim. Cosmochim. Acta* **70**, 4130–4139.
- Achterberg E. P., Herzi V. M. C., Braungardt C. B. and Millward G. E. (2003) Metal behaviour in an estuary polluted by acid mine drainage: The role of particulate matter. *Environ. Pollut.* **121**, 283–292.
- Amaral V., Romera-Castillo C., García-Delgado M., Gómez-Parra A. and Forja J. (2020) Distribution of dissolved organic matter in estuaries of the southern Iberian Atlantic Basin: Sources, behavior and export to the coastal zone. *Mar. Chem.* **226**, 103857.

- Araújo D. F., Boaventura G. R., Machado W., Viers J., Weiss D., Patchineelam S. R., Ruiz I., Rodrigues A. P. C., Babinski M. and Dantas E. (2017) Tracing of anthropogenic zinc sources in coastal environments using stable isotope composition. *Chem. Geol.* **449**, 226–235. Available at: <http://dx.doi.org/10.1016/j.chemgeo.2016.12.004>.
- Araújo D. F., Knoery J., Briant N., Vigier N. and Ponzevera E. (2022) “Non-traditional” stable isotopes applied to the study of trace metal contaminants in anthropized marine environments. *Mar. Pollut. Bull.* **175**, 113398.
- Archer C. (2007) The application of transition metal isotope systems to biogeochemical studies of the early Earth. University of London.
- Archer C., Andersen M. B., Cloquet C., Conway T. M., Dong S., Ellwood M. J., Moore R., Nelson J., Rehkämper M., Rouxel O., Samanta M., Shin K.-C. C., Sohrin Y., Takano S. and Wasylenki L. E. (2017) Inter-calibration of a proposed new primary reference standard AA-ETH Zn for zinc isotopic analysis. *J. Anal. At. Spectrom.* **32**, 415–419.
- Archer C. and Vance D. (2004) Mass discrimination correction in multiple-collector plasma source mass spectrometry: an example using Cu and Zn isotopes. *J. Anal. At. Spectrom.* **19**, 656.
- Arnold T., Schönbächler M., Rehkämper M., Dong S., Zhao F. J., Kirk G. J. D., Coles B. J. and Weiss D. J. (2010) Measurement of zinc stable isotope ratios in biogeochemical matrices by double-spike MC-ICPMS and determination of the isotope ratio pool available for plants from soil. *Anal. Bioanal. Chem.* **398**, 3115–3125.
- Asghari I., Mousavi S. M., Amiri F. and Tavassoli S. (2013) Bioleaching of spent refinery catalysts: A review. *J. Ind. Eng. Chem.* **19**, 1069–1081.
- Balistrieri L. S., Borrok D. M., Wanty R. B. and Ridley W. I. (2008) Fractionation of Cu and Zn isotopes during adsorption onto amorphous Fe(III) oxyhydroxide: Experimental mixing of acid rock drainage and ambient river water. *Geochim. Cosmochim. Acta* **72**, 311–328.
- Balistrieri L. S. and Murray J. W. (1982) The adsorption of Cu, Pb, Zn, and Cd on goethite from major ion seawater. *Geochim. Cosmochim. Acta* **46**, 1253–1265.
- Barba-Brioso C., Fernández-Caliani J. C., Miras A., Cornejo J. and Galán E. (2010) Multi-source water pollution in a highly anthropized wetland system associated with the estuary of Huelva (SW Spain). *Mar. Pollut. Bull.* **60**, 1259–1269.
- Bigham J. M., Schwertmann U., Traina S. J., Winland R. L. and Wolf M. (1996) Schwertmannite and the chemical modeling of iron in acid sulfate waters. *Geochim. Cosmochim. Acta* **60**, 2111–2121.
- Bonnissel-Gissinger P., Alnot M., Ehrhardt J. J. and Behra P. (1998) Surface oxidation of pyrite as a function of pH. *Environ. Sci. Technol.* **32**, 2839–2845.
- Borrego J., Morales J. A. and Pendon J. G. (1995) Holocene estuarine facies along the mesotidal coast of Huelva, south-western Spain. *Tidal signatures Mod. Anc. sediments*, 151–170.
- Borrok D. M., Nimick D. A., Wanty R. B. and Ridley W. I. (2008) Isotopic variations of dissolved copper and zinc in stream waters affected by historical mining. *Geochim. Cosmochim. Acta* **72**, 329–344.
- Boyle E. A., Huested S. S. and Grant B. (1982) The chemical mass balance of the amazon plume-II. Copper, nickel, and cadmium. *Deep Sea Res. Part A, Oceanogr. Res. Pap.* **29**, 1355–1364.
- Boyle E. A., John S. G., Abouchami W., Adkins J. F., Echegoyen-Sanz Y., Ellwood M. J., Flegal A. R., Fornace K., Gallon C., Galer S. J. G., Gault-Ringold M., Lacan F., Radic A., Rehkämper M., Rouxel O., Sohrin Y., Stirling C., Thompson C., Vance D., Xue Z. and Zhao Y. (2012) GEOTRACES IC1 (BATS) contamination-prone trace element isotopes Cd, Fe, Pb, Zn, Cu, and Mo intercalibration. *Limnol.*

- Braungardt C. B., Achterberg E. P., Elbaz-Poulichet F. and Morley N. H. (2003) Metal geochemistry in a mine-polluted estuarine system in Spain. *Appl. Geochemistry* **18**, 1757–1771.
- Bridgestock L. J., Williams H., Rehkämper M., Larnier F., Giscard M. D., Hammond S., Coles B. J., Andreasen R., Wood B. J. and Theis K. J. (2014) Unlocking the zinc isotope systematics of iron meteorites. *Earth Planet. Sci. Lett.* **400**, 153–164.
- Bruland K. W., Middag R. and Lohan M. C. (2013) *Controls of Trace Metals in Seawater*. 2nd ed., Elsevier Ltd.
- Bryan A. L., Dickson A. J., Dowdall F., Homoky W. B., Porcelli D. and Henderson G. M. (2021) Controls on the cadmium isotope composition of modern marine sediments. *Earth Planet. Sci. Lett.* **565**, 116946.
- Bryan A. L., Dong S., Wilkes E. B. and Wasylenki L. E. (2015) Zinc isotope fractionation during adsorption onto Mn oxyhydroxide at low and high ionic strength. *Geochim. Cosmochim. Acta* **157**, 182–197.
- Buckby T., Black S., Coleman M. L. and Hodson M. E. (2003) Fe-sulphate-rich evaporative mineral precipitates from the Río Tinto, southwest Spain. *Mineral. Mag.* **67**, 263–278.
- Burchard H., Schuttelaars H. M. and Ralston D. K. (2018) Sediment trapping in estuaries. *Ann. Rev. Mar. Sci.* **10**, 371–395.
- Cánovas C. R., Olías M., Nieto J. M. and Galván L. (2010) Wash-out processes of evaporitic sulfate salts in the Tinto river: Hydrogeochemical evolution and environmental impact. *Appl. Geochemistry* **25**, 288–301.
- Cánovas C. R., Olías M., Nieto J. M., Sarmiento A. M. and Cerón J. C. (2007) Hydrogeochemical characteristics of the Tinto and Odiel Rivers (SW Spain). Factors controlling metal contents. *Sci. Total Environ.* **373**, 363–382.
- Chapman J. B., Mason T. F. D., Weiss D. J., Coles B. J. and Wilkinson J. J. (2006) Chemical separation and isotopic variations of Cu and Zn from five geological reference materials. *Geostand. Geoanalytical Res.* **30**, 5–16.
- Chen J., Gaillardet J. and Louvat P. (2008) Zinc isotopes in the Seine River waters, France: A probe of anthropogenic contamination. *Environ. Sci. Technol.* **42**, 6494–6501.
- Chen L., Little S. H., Kreissig K., Severmann S. and Mcmanus J. (2021) Isotopically Light Cd in Sediments Underlying Oxygen Deficient Zones. *Front. Earth Sci.* **9**.
- Chester R. and Jickells T. (2012) *Marine Geochemistry*, John Wiley and Sons.
- Cloquet C., Carignan J., Libourel G., Sterckeman T. and Perdrix E. (2006) Tracing source pollution in soils using cadmium and lead isotopes. *Environ. Sci. Technol.* **40**, 2525–2530.
- Conway T. M. and John S. G. (2015) Biogeochemical cycling of cadmium isotopes along a high-resolution section through the North Atlantic Ocean. *Geochim. Cosmochim. Acta* **148**, 269–283.
- Conway T. M. and John S. G. (2014) The biogeochemical cycling of zinc and zinc isotopes in the North Atlantic Ocean. *Global Biogeochem. Cycles* **28**, 1111–1128.
- Conway T. M., Rosenberg A. D., Adkins J. F. and John S. G. (2013) A new method for precise determination of iron, zinc and cadmium stable isotope ratios in seawater by double-spike mass spectrometry. *Anal. Chim. Acta* **793**, 44–52.
- Costa O. Y. A., Oguejiofor C., Zühlke D., Barreto C. C., Wünsche C., Riedel K. and Kuramae E. E. (2020) Impact of Different Trace Elements on the Growth and Proteome of Two Strains of *Granulicella*, Class “Acidobacteria.” *Front. Microbiol.* **11**, 1–16.

- Dabrin A., Schäfer J., Blanc G., Strady E., Masson M., Bossy C., Castelle S., Girardot N. and Coynel A. (2009) Improving estuarine net flux estimates for dissolved cadmium export at the annual timescale: Application to the Gironde Estuary. *Estuar. Coast. Shelf Sci.* **84**, 429–439.
- Dai M. H. and Martin J. M. (1995) First data on trace metal level and behaviour in two major Arctic river-estuarine systems (Ob and Yenisey) and in the adjacent Kara Sea, Russia. *Earth Planet. Sci. Lett.* **131**, 127–141.
- Desaulty A. M. and Petelet-Giraud E. (2020) Zinc isotope composition as a tool for tracing sources and fate of metal contaminants in rivers. *Sci. Total Environ.* **728**, 138599.
- Dong S., Ochoa Gonzalez R., Harrison R. M., Green D., North R., Fowler G. and Weiss D. (2017) Isotopic signatures suggest important contributions from recycled gasoline, road dust and non-exhaust traffic sources for copper, zinc and lead in PM10 in London, United Kingdom. *Atmos. Environ.* **165**, 88–98.
- Dong S. and Wasylenki L. E. (2016) Zinc isotope fractionation during adsorption to calcite at high and low ionic strength. *Chem. Geol.* **447**, 70–78.
- Edmond J. M., Spivack A., Grant B. C., Ming-Hui H., Chen Z., Chen S. and Zeng X. (1985) Chemical dynamics of the Changjiang estuary. *Cont. Shelf Res.* **4**, 17–36.
- Edwards K. J., Gihring T. M. and Banfield J. F. (1999) Seasonal variations in microbial populations and environmental conditions in an extreme acid mine drainage environment. *Appl. Environ. Microbiol.* **65**, 3627–3632.
- Elbaz-Poulichet F., Garnier J. M., Guan D. M., Martin J. M. and Thomas A. J. (1996) The conservative behaviour of trace metals (Cd, Cu, Ni and Pb) and as in the surface plume of stratified estuaries: Example of the Rhone river (France). *Estuar. Coast. Shelf Sci.* **42**, 289–310.
- Elbaz-Poulichet F., Guieu C. and Morley N. H. (2001a) A reassessment of trace metal budgets in the western Mediterranean Sea. *Mar. Pollut. Bull.* **42**, 623–627.
- Elbaz-Poulichet F., Martin J. M., Huang W. W. and Zhu J. X. (1987) Dissolved Cd behaviour in some selected french and chinese estuaries. Consequences on Cd supply to the ocean. *Mar. Chem.* **22**, 125–136.
- Elbaz-Poulichet F., Morley N. H., Beckers J. M. and Nomerange P. (2001b) Metal fluxes through the strait of gibraltar: The influence of the tinto and odiel rivers (sw spain). *Mar. Chem.* **73**, 193–213.
- Elliott M. and McLusky D. S. (2002) The need for definitions in understanding estuaries. *Estuar. Coast. Shelf Sci.* **55**, 815–827.
- España J. S., López Pamo E., Santofimia Pastor E., Reyes Andrés J. and Martín Rubí J. A. (2006) The removal of dissolved metals by hydroxysulphate precipitates during oxidation and neutralization of acid mine waters, Iberian Pyrite Belt. *Aquat. Geochemistry* **12**, 269–298.
- España J. S., Pamo E. L., Pastor E. S., Andrés J. R. and Rubí J. A. M. (2005a) The natural attenuation of two acidic effluents in Tharsis and La Zarza-Perrunal mines (Iberian Pyrite Belt, Huelva, Spain). *Environ. Geol.* **49**, 253–266.
- España J. S., Pamo E. L., Santofimia E., Aduvire O., Reyes J. and Baretino D. (2005b) Acid mine drainage in the Iberian Pyrite Belt (Odiel river watershed, Huelva, SW Spain): Geochemistry, mineralogy and environmental implications. *Appl. Geochemistry* **20**, 1320–1356.
- Fairbrother A., Wenstel R., Sappington K. and Wood W. (2007) Framework for Metals Risk Assessment. *Ecotoxicol. Environ. Saf.* **68**, 145–227.
- Fan C., Guo C., Chen M., Huang W., Wan J., Reinfelder J. R., Li X., Zeng Y., Lu G. and Dang Z. (2019)

- Fang T., Wang H., Liang Y., Cui K., Yang K., Lu W., Li J., Zhao X., Gao N., Yu Q., Li H. and Jiang H. (2022) Source tracing with cadmium isotope and risk assessment of heavy metals in sediment of an urban river, China. *Environ. Pollut.* **305**, 119325.
- Fernandez A. and Borrok D. M. (2009) Fractionation of Cu, Fe, and Zn isotopes during the oxidative weathering of sulfide-rich rocks. *Chem. Geol.* **264**, 1–12.
- Fujii T., Moynier F., Pons M. L. and Albarède F. (2011) The origin of Zn isotope fractionation in sulfides. *Geochim. Cosmochim. Acta* **75**, 7632–7643.
- Gaillardet J., Viers J. and Dupre B. (2003) Trace Elements in River Waters. In *Treatise on Geochemistry* (eds. H. D. Holland and K. K. Turekian). Pergamon, Oxford. pp. 225–272.
- Gao B., Zhou H., Liang X. and Tu X. (2013) Cd isotopes as a potential source tracer of metal pollution in river sediments. *Environ. Pollut.* **181**, 340–343.
- Garel E., Laiz I., Drago T. and Relvas P. (2016) Characterisation of coastal counter-currents on the inner shelf of the Gulf of Cadiz. *J. Mar. Syst.* **155**, 19–34.
- Van Geen A., Adkins J. F., Boyle E. A., Nelson C. H. and Palanques A. (1997) A120 yr record of widespread contamination from mining of the Iberian pyrite belt. *Geology* **25**, 291–294.
- Van Geen A. and Boyle E. A. (1990) Variability of trace-metal fluxes through the Strait of Gibraltar. *Glob. Planet. Change* **3**, 65–79.
- Van Geen A., Boyle E. A. and Moore W. S. (1991) Trace metal enrichments in waters of the Gulf of Cadiz, Spain. *Geochim. Cosmochim. Acta* **55**, 2173–2191.
- Van Geen A., Rosener P. and Boyle E. A. (1988) Entrainment of trace-metal-enriched Atlantic-shelf water in the inflow to the Mediterranean Sea. *Nature* **331**, 423–426.
- Gélabert A., Pokrovsky O. S., Viers J., Schott J., Boudou A. and Feurtet-Mazel A. (2006) Interaction between zinc and freshwater and marine diatom species: Surface complexation and Zn isotope fractionation. *Geochim. Cosmochim. Acta* **70**, 839–857.
- Gelly R., Fekiacova Z., Guihou A., Doelsch E., Deschamps P. and Keller C. (2019) Lead, zinc, and copper redistributions in soils along a deposition gradient from emissions of a Pb-Ag smelter decommissioned 100 years ago. *Sci. Total Environ.* **665**, 502–512.
- Gong W. and Shen J. (2011) The response of salt intrusion to changes in river discharge and tidal mixing during the dry season in the Modaomen Estuary, China. *Cont. Shelf Res.* **31**, 769–788.
- Gonzalez R. O., Strekopytov S., Amato F., Querol X., Reche C. and Weiss D. (2016) New Insights from Zinc and Copper Isotopic Compositions into the Sources of Atmospheric Particulate Matter from Two Major European Cities. *Environ. Sci. Technol.* **50**, 9816–9824.
- Gou W., Li W., Ji J. and Li W. (2018) Zinc Isotope Fractionation during Sorption onto Al Oxides: Atomic Level Understanding from EXAFS. *Environ. Sci. Technol.* **52**, 9087–9096.
- Griffiths A., Packman H., Leung Y. L., Coles B. J., Kreissig K., Little S. H., Van De Fliedert T. and Rehkämper M. (2020) Evaluation of Optimized Procedures for High-Precision Lead Isotope Analyses of Seawater by Multiple Collector Inductively Coupled Plasma Mass Spectrometry. *Anal. Chem.* **92**, 11232–11241.
- Guerrero J. L., Gutiérrez-Álvarez I., Mosqueda F., Olías M., García-Tenorio R. and Bolívar J. P. (2019) Pollution evaluation on the salt-marshes under the phosphogypsum stacks of Huelva due to deep leachates. *Chemosphere* **230**, 219–229.
- Guerrero J. L., Pérez-Moreno S. M., Gutiérrez-Álvarez I., Gázquez M. J. and Bolívar J. P. (2021) Behaviour

- Guinoiseau D., Bouchez J., Gélabert A., Louvat P., Moreira-Turcq P., Filizola N. and Benedetti M. F. (2018a) Fate of particulate copper and zinc isotopes at the Solimões-Negro river confluence, Amazon Basin, Brazil. *Chem. Geol.* **489**, 1–15.
- Guinoiseau D., Galer S. J. G. and Abouchami W. (2018b) Effect of cadmium sulphide precipitation on the partitioning of Cd isotopes: Implications for the oceanic Cd cycle. *Earth Planet. Sci. Lett.* **498**, 300–308.
- Gzyl G. and Banks D. (2007) Verification of the “first flush” phenomenon in mine water from coal mines in the Upper Silesian Coal Basin, Poland. *J. Contam. Hydrol.* **92**, 66–86.
- Hierro A., Olías M., Ketterer M. E., Vaca F., Borrego J., Cánovas C. R. and Bolivar J. P. (2014) Geochemical behavior of metals and metalloids in an estuary affected by acid mine drainage (AMD). *Environ. Sci. Pollut. Res.* **21**, 2611–2627.
- Horner T. J., Little S. H., Conway T. M., Farmer J. R., Hertzberg J. E., Janssen D. J., Lough A. J. M., McKay J. L., Tessin A., Galer S. J. G., Jaccard S. L., Lacan F., Paytan A. and Wuttig K. (2021) Bioactive Trace Metals and Their Isotopes as Paleoproductivity Proxies: An Assessment Using GEOTRACES-Era Data. *Global Biogeochem. Cycles* **35**, e2020GB006814.
- Horner T. J., Rickaby R. E. M. and Henderson G. M. (2011) Isotopic fractionation of cadmium into calcite. *Geochemistry, Geophys. Geosystems* **312**, 243–253.
- John S. G. and Conway T. M. (2014) A role for scavenging in the marine biogeochemical cycling of zinc and zinc isotopes. *Earth Planet. Sci. Lett.* **394**, 159–167.
- John S. G., Geis R. W., Saito M. A. and Boyle E. A. (2007) Zinc isotope fractionation during high affinity and low-affinity zinc transport by the marine diatom *Thalassiosira oceanica*. *Limnol. Oceanogr.* **52**, 2710–2714.
- John S. G., Helgoe J., Townsend E., Weber T., DeVries T., Tagliabue A., Moore K., Lam P., Marsay C. M. and Till C. (2018) Biogeochemical cycling of Zn and Cd and their stable isotopes in the Eastern Tropical South Pacific. *Mar. Chem.* **201**, 256–262.
- John S. G., Rouxel O. J., Craddock P. R., Engwall A. M. and Boyle E. A. (2008) Zinc stable isotopes in seafloor hydrothermal vent fluids and chimneys. *Earth Planet. Sci. Lett.* **269**, 17–28.
- Johnson D. B. and Hallberg K. B. (2005) Acid mine drainage remediation options: A review. *Sci. Total Environ.* **338**, 3–14.
- Jönsson J., Persson P., Sjöberg S. and Lövgren L. (2005) Schwertmannite precipitated from acid mine drainage: Phase transformation, sulphate release and surface properties. *Appl. Geochemistry* **20**, 179–191.
- Jouvin D., Louvat P., Juillot F., Maréchal C. N. and Benedetti M. F. (2009) Zinc isotopic fractionation: Why organic matters. *Environ. Sci. Technol.* **43**, 5747–5754.
- Juillot F., Maréchal C., Ponthieu M., Cacaly S., Morin G., Benedetti M., Hazemann J. L., Proux O. and Guyot F. (2008) Zn isotopic fractionation caused by sorption on goethite and 2-Lines ferrihydrite. *Geochim. Cosmochim. Acta* **72**, 4886–4900.
- Kafantaris F. C. A. and Borrok D. M. (2014) Zinc isotope fractionation during surface adsorption and intracellular incorporation by bacteria. *Chem. Geol.* **366**, 42–51.
- Köbberich M. and Vance D. (2017) Kinetic control on Zn isotope signatures recorded in marine diatoms. *Geochim. Cosmochim. Acta* **210**, 97–113.
- Köbberich M. and Vance D. (2019) Zn isotope fractionation during uptake into marine phytoplankton: Implications for oceanic zinc isotopes. *Chem. Geol.* **523**, 154–161.



- Laiz I., Plecha S., Teles-Machado A., González-Ortegón E., Sánchez-Quiles D., Cobelo-García A., Roque D., Peliz A., Sánchez-Leal R. F. and Tovar-Sánchez A. (2020) The role of the Gulf of Cadiz circulation in the redistribution of trace metals between the Atlantic Ocean and the Mediterranean Sea. *Sci. Total Environ.* **719**, 134964.
- Lambelet M., Rehkämper M., van de Flierdt T., Xue Z., Kreissig K., Coles B., Porcelli D. and Andersson P. (2013) Isotopic analysis of Cd in the mixing zone of Siberian rivers with the Arctic Ocean-New constraints on marine Cd cycling and the isotope composition of riverine Cd. *Earth Planet. Sci. Lett.* **361**, 64–73.
- Larner F. and Rehkämper M. (2012) Evaluation of Stable Isotope Tracing for ZnO Nanomaterials: New Constraints from High Precision Isotope Analyses and Modeling. *Environ. Sci. Technol.* **46**, 4149–4158.
- Leistel J. M., Marcoux E., Thiéblemont D., Quesada C., Sánchez A., Almodóvar G. R., Pascual E. and Sáez R. (1997) The volcanic-hosted massive sulphide deposits of the Iberian Pyrite Belt: Review and preface to the Thematic Issue. *Miner. Depos.* **33**, 2–30.
- Little S. H., Munson S., Prytulak J., Coles B. J., Hammond S. J. and Widdowson M. (2019) Cu and Zn isotope fractionation during extreme chemical weathering. *Geochim. Cosmochim. Acta* **263**, 85–107.
- Little S. H., Vance D., McManus J. and Severmann S. (2016) Key role of continental margin sediments in the oceanic mass balance of Zn and Zn isotopes. *Geology* **44**, 207–210.
- Little S. H., Vance D., Walker-Brown C. and Landing W. M. (2014) The oceanic mass balance of copper and zinc isotopes, investigated by analysis of their inputs, and outputs to ferromanganese oxide sediments. *Geochim. Cosmochim. Acta* **125**, 673–693.
- Liu Y., Gao T., Xia Y., Wang Z., Liu C., Li S., Wu Q., Qi M. and Lv Y. (2020) Using Zn isotopes to trace Zn sources and migration pathways in paddy soils around mining area. *Environ. Pollut.* **267**, 115616.
- Maréchal C. N., Télouk P. and Albarède F. (1999) Precise analysis of copper and zinc isotopic compositions by plasma-source mass spectrometry. *Chem. Geol.* **156**, 251–273.
- Martin D. F., Dooris P. M. and Sumpter D. (2001) Environmental impacts of phosphogypsum vs. borrow pits in roadfill construction. *J. Environ. Sci. Heal. - Part A Toxic/Hazardous Subst. Environ. Eng.* **36**, 1975–1982.
- Martín J. E., García-Tenorio R., San Miguel E. G., Respaldiza M. Á., Bolívar J. P., Alves L. C. and Da Silva M. F. (2002) Historical impact in an estuary of some mining and industrial activities evaluated through the analysis by TPIXE of a dated sediment core. In *Nuclear Instruments and Methods in Physics Research, Section B: Beam Interactions with Materials and Atoms* pp. 153–157.
- Mason T. F. D., Weiss D. J., Chapman J. B., Wilkinson J. J., Tessalina S. G., Spiro B., Horstwood M. S. A., Spratt J. and Coles B. J. (2005) Zn and Cu isotopic variability in the Alexandrinka volcanic-hosted massive sulphide (VHMS) ore deposit, Urals, Russia. *Chem. Geol.* **221**, 170–187.
- Matthies R., Sinclair S. A. and Blowes D. W. (2014) The zinc stable isotope signature of waste rock drainage in the Canadian permafrost region. *Appl. Geochemistry* **48**, 53–57.
- Mavromatis V., González A. G., Dietzel M. and Schott J. (2019) Zinc isotope fractionation during the inorganic precipitation of calcite – Towards a new pH proxy. *Geochim. Cosmochim. Acta* **244**, 99–112.
- Meade R. H. (1969) Landward Transport of Bottom Sediments in Estuaries of the Atlantic Coastal Plain. *J. Sediment. Res.* **Vol. 39**, 222–234.
- Mielke R. E., Pace D. L., Porter T. and Southam G. (2003) A critical stage in the formation of acid mine drainage: Colonization of pyrite by *Acidithiobacillus ferrooxidans* under pH-neutral conditions. *Geobiology* **1**, 81–90.

Molinas E., Vinzon S. B., de Paula Xavier Vilela C. and Gallo M. N. (2014) Structure and position of the bottom salinity front in the Amazon Estuary. *Ocean Dyn.* **64**, 1583–1599.

Moore R. E. T., Ullah I., de Oliveira V. H., Hammond S. J., Strekopytov S., Tibbett M., Dunwell J. M. and Rehkämper M. (2020) Cadmium isotope fractionation reveals genetic variation in Cd uptake and translocation by *Theobroma cacao* and role of natural resistance-associated macrophage protein 5 and heavy metal ATPase-family transporters. *Hortic. Res.* **7**, 71.

Morel F. M. M. and Price N. M. (2003) The biogeochemical cycles of trace metals in the oceans. *Science* (80- ). **300**, 944–947.

Moynier F., Vance D., Fujii T. and Savage P. (2017) The Isotope Geochemistry of Zinc and Copper. *Rev. Mineral. Geochemistry* **82**, 543–600.

Mulero-Martínez R., Gómez-Enri J., Mañanes R. and Bruno M. (2021) Assessment of near-shore currents from CryoSat-2 satellite in the Gulf of Cádiz using HF radar-derived current observations. *Remote Sens. Environ.* **256**.

Murphy K., Rehkämper M., Kreissig K., Coles B. J. and van de Fliert T. (2016) Improvements in Cd stable isotope analysis achieved through use of liquid–liquid extraction to remove organic residues from Cd separates obtained by extraction chromatography. *J. Anal. At. Spectrom.* **31**, 319–327.

Muysen B. T. A., De Schamphelaere K. A. C. and Janssen C. R. (2006) Mechanisms of chronic waterborne Zn toxicity in *Daphnia magna*. *Aquat. Toxicol.* **77**, 393–401.

Nieto J. M., Sarmiento A. M., Cánovas C. R., Olías M. and Ayora C. (2013) Acid mine drainage in the Iberian Pyrite Belt: 1. Hydrochemical characteristics and pollutant load of the Tinto and Odiel rivers. *Environ. Sci. Pollut. Res.* **20**, 7509–7519.

Nocete F., Alex E., Nieto J. M., Sáez R. and Bayona M. R. (2005) An archaeological approach to regional environmental pollution in the south-western Iberian Peninsula related to Third millennium BC mining and metallurgy. *J. Archaeol. Sci.* **32**, 1566–1576.

Nordstrom D. K. (2011) Hydrogeochemical processes governing the origin, transport and fate of major and trace elements from mine wastes and mineralized rock to surface waters. *Appl. Geochemistry* **26**, 1777–1791.

Nriagu J. O. and Pacyna J. M. (1988) Quantitative assessment of worldwide contamination of air, water and soils by trace metals. *Nature* **333**, 134–139.

Olías M., Cánovas C. R., Basallote M. D., Macías F., Pérez-López R., González R. M., Millán-Becerro R. and Nieto J. M. (2019) Causes and impacts of a mine water spill from an acidic pit lake (Iberian Pyrite Belt). *Environ. Pollut.* **250**, 127–136.

Olías M., Cánovas C. R., Nieto J. M. and Sarmiento A. M. (2006) Evaluation of the dissolved contaminant load transported by the Tinto and Odiel rivers (South West Spain). *Appl. Geochemistry* **21**, 1733–1749.

Olías M., Nieto J. M., Sarmiento A. M., Cerón J. C. and Cánovas C. R. (2004) Seasonal water quality variations in a river affected by acid mine drainage: The Odiel River (South West Spain). *Sci. Total Environ.* **333**, 267–281.

Paalman M. A. A., Van Der Weijden C. H. and Loch J. P. G. (1994) Sorption of cadmium on suspended matter under estuarine conditions; competition and complexation with major sea-water ions. *Water, Air, Soil Pollut.* **73**, 49–60.

Pacyna J. M. and Pacyna E. G. (2001) An assessment of global and regional emissions of trace metals to the atmosphere from anthropogenic sources worldwide. *Environ. Rev.* **9**, 269–298.

- Papaslioti E. M., Pérez-López R., Parviainen A., Macías F., Delgado-Huertas A., Garrido C. J., Marchesi C. and Nieto J. M. (2018) Stable isotope insights into the weathering processes of a phosphogypsum disposal area. *Water Res.* **140**, 344–353.
- Pattanaik A., Sukla L. B., Pradhan D. and Krishna Samal D. P. (2020) Microbial mechanism of metal sulfide dissolution. *Mater. Today Proc.* **30**, 326–331.
- Peliz A., Marchesiello P., Santos A. M. P., Dubert J., Teles-Machado A., Marta-Almeida M. and Le Cann B. (2009) Surface circulation in the Gulf of Cadiz: 2. Inflow-outflow coupling and the Gulf of Cadiz slope current. *J. Geophys. Res. Ocean.* **114**.
- Pérez-López R., Álvarez-Valero A. M. and Nieto J. M. (2007) Changes in mobility of toxic elements during the production of phosphoric acid in the fertilizer industry of Huelva (SW Spain) and environmental impact of phosphogypsum wastes. *J. Hazard. Mater.* **148**, 745–750.
- Pérez-López R., Macías F., Cánovas C. R., Sarmiento A. M. and Pérez-Moreno S. M. (2016) Pollutant flows from a phosphogypsum disposal area to an estuarine environment: An insight from geochemical signatures. *Sci. Total Environ.* **553**, 42–51.
- Pérez-López R., Nieto J. M., de la Rosa J. D. and Bolívar J. P. (2015) Environmental tracers for elucidating the weathering process in a phosphogypsum disposal site: Implications for restoration. *J. Hydrol.* **529**, 1313–1323.
- Pérez-López R., Nieto J. M., López-Cascajosa M. J., Díaz-Blanco M. J., Sarmiento A. M., Oliveira V. and Sánchez-Rodas D. (2011) Evaluation of heavy metals and arsenic speciation discharged by the industrial activity on the Tinto-Odiel estuary, SW Spain. *Mar. Pollut. Bull.* **62**, 405–411.
- Pérez-López R., Nieto J. M., López-Coto I., Aguado J. L., Bolívar J. P. and Santisteban M. (2010) Dynamics of contaminants in phosphogypsum of the fertilizer industry of Huelva (SW Spain): From phosphate rock ore to the environment. *Appl. Geochemistry* **25**, 705–715.
- Petit J. C. J., Schäfer J., Coynel A., Blanc G., Chiffolleau J. F., Auger D., Bossy C., Derriennic H., Mikolaczyk M., Dutruch L. and Mattielli N. (2015) The estuarine geochemical reactivity of Zn isotopes and its relevance for the biomonitoring of anthropogenic Zn and Cd contaminations from metallurgical activities: Example of the Gironde fluvial-estuarine system, France. *Geochim. Cosmochim. Acta* **170**, 108–125.
- Plumlee G. S., Logsdon M. J. and Filipek L. F. (2020) *The Environmental Geochemistry of Mineral Deposits.*, Society of economic geologists, inc.
- Pokrovsky O. S., Viers J. and Freyrier R. (2005) Zinc stable isotope fractionation during its adsorption on oxides and hydroxides. *J. Colloid Interface Sci.* **291**, 192–200.
- Querol X., Alastuey A., De La Rosa J., Sánchez-De-La-Campa A., Plana F. and Ruiz C. R. (2002) Source apportionment analysis of atmospheric particulates in an industrialised urban site in southwestern Spain. *Atmos. Environ.* **36**, 3113–3125.
- Randall S. R., Sherman D. M., Ragnarsdottir K. V. and Collins C. R. (1999) The mechanism of cadmium surface complexation on iron oxyhydroxide minerals. *Geochim. Cosmochim. Acta* **63**, 2971–2987.
- Ratié G., Chrastný V., Guinoiseau D., Marsac R., Vaňková Z. and Komárek M. (2021) Cadmium Isotope Fractionation during Complexation with Humic Acid. *Environ. Sci. Technol.* **55**, 7430–7444.
- Rauch J. N. and Pacyna J. M. (2009) Earth's global Ag, Al, Cr, Cu, Fe, Ni, Pb, and Zn cycles. *Global Biogeochem. Cycles* **23**, 1–16.
- Rentería-Villalobos M., Vioque I., Mantero J. and Manjón G. (2010) Radiological, chemical and morphological characterizations of phosphate rock and phosphogypsum from phosphoric acid factories in SW Spain. *J. Hazard. Mater.* **181**, 193–203.

- Roshan S., DeVries T., Wu J. and Chen G. (2018) The Internal Cycling of Zinc in the Ocean. *Global Biogeochem. Cycles* **32**, 1833–1849.
- Rudnick R. L. and Gao S. (2003) 3.01 - Composition of the Continental Crust. *Treatise on Geochemistry* **1**, 1–64.
- Sáez R., Pascual E., Toscano M. and Almodóvar G. R. (1999) The Iberian type of volcano-sedimentary massive sulphide deposits. *Miner. Depos.* **34**, 549–570.
- Sainz A., Grande J. A. and de la Torre M. L. (2004) Characterisation of heavy metal discharge into the Ria of Huelva. *Environ. Int.* **30**, 557–566.
- Sarmiento A. M., Nieto J. M., Olías M. and Cánovas C. R. (2009) Hydrochemical characteristics and seasonal influence on the pollution by acid mine drainage in the Odiel river Basin (SW Spain). *Appl. Geochemistry* **24**, 697–714.
- Schleicher N. J., Dong S., Packman H., Little S. H., Ochoa Gonzalez R., Najorka J., Sun Y. and Weiss D. J. (2020) A Global Assessment of Copper, Zinc, and Lead Isotopes in Mineral Dust Sources and Aerosols. *Front. Earth Sci.* **8**, 1–20.
- Schlitzer R., Anderson R. F., Dodas E. M., Lohan M., Geibert W., Tagliabue A., Bowie A., Jeandel C., Maldonado M. T., Landing W. M., Cockwell D., Abadie C., Abouchami W., Achterberg E. P., Agather A., Aguiar-Islas A., van Aken H. M., Andersen M., Archer C., Auro M., de Baar H. J. W., Baars O., Baker A. R., Bakker K., Basak C., Baskaran M., Bates N. R., Bauch D., van Beek P., Behrens M. K., Black E., Bluhm K., Bopp L., Bouman H., Bowman K., Bown J., Boyd P., Boye M., Boyle E. A., Branellec P., Bridgestock L., Brissebrat G., Browning T., Bruland K. W., Brumsack H. J., Brzezinski M., Buck C. S., Buck K. N., Buesseler K., Bull A., Butler E., Cai P., Mor P. C., Cardinal D., Carlson C., Carrasco G., Casacuberta N., Casciotti K. L., Castrillejo M., Chamizo E., Chance R., Charette M. A., Chaves J. E., Cheng H., Chever F., Christl M., Church T. M., Closset I., Colman A., Conway T. M., Cossa D., Croft P., Cullen J. T., Cutter G. A., Daniels C., Dehairs F., Deng F., Dieu H. T., Duggan B., Dulaquais G., Dumousseaud C., Echegoyen-Sanz Y., Edwards R. L., Ellwood M. J., Fahrback E., Fitzsimmons J. N., Russell Flegal A., Fleisher M. Q., van de Flierdt T., Frank M., Friedrich J., Fripiat F., Fröllje H., Galer S. J. G., Gamo T., Ganeshram R. S., Garcia-Orellana J., Garcia-Solsona E., Gault-Ringold M., George E., Gerringa L. J. A., Gilbert M., Godoy J. M., Goldstein S. L., Gonzalez S. R., Grissom K., Hammerschmidt C., Hartman A., Hassler C. S., Hathorne E. C., Hatta M., Hawco N., Hayes C. T., Heimbürger L. E., Helgoe J., Heller M., Henderson G. M., Henderson P. B., van Heuven S., Ho P., Horner T. J., Hsieh Y. Te, Huang K. F., Humphreys M. P., Isshiki K., Jacquot J. E., Janssen D. J., Jenkins W. J., John S. G., Jones E. M., Jones J. L., Kadko D. C., Kayser R., Kenna T. C., Khondoker R., Kim T., Kipp L., Klar J. K., Klunder M., Kretschmer S., Kumamoto Y., Laan P., Labatut M., Lacan F., Lam P. J., Lambelet M., Lamborg C. H., Le Moigne F. A. C., Le Roy E., Lechtenfeld O. J., Lee J. M., Lherminier P., Little S. H., López-Lora M., Lu Y., Masque P., Mawji E., McClain C. R., Measures C., Mehic S., Barraqueta J. L. M., van der Merwe P., Middag R., Mieruch S., Milne A., Minami T., Moffett J. W., Moncoiffe G., Moore W. S., Morris P. J., Morton P. L., Nakaguchi Y., Nakayama N., Niedermiller J., Nishioka J., Nishiuchi A., Noble A., Obata H., Ober S., Ohnemus D. C., van Ooijen J., O'Sullivan J., Owens S., Pahnke K., Paul M., Pavia F., Pena L. D., Peters B., Planchon F., Planquette H., Pradoux C., Puigcorbé V., Quay P., Queroue F., Radic A., Rauschenberg S., Rehkämper M., Rember R., Remenyi T., Resing J. A., Rickli J., Rigaud S., Rijkenberg M. J. A., Rintoul S., Robinson L. F., Roca-Martí M., Rodellas V., Roeske T., Rolison J. M., Rosenberg M., Roshan S., Rutgers van der Loeff M. M., Ryabenko E., Saito M. A., Salt L. A., Sanial V., Sarthou G., Schallenberg C., Schauer U., Scher H., Schlosser C., Schnetger B., Scott P., Sedwick P. N., Semiletov I., Shelley R., Sherrell R. M., Shiller A. M., Sigman D. M., Singh S. K., Slagter H. A., Slater E., Smethie W. M., Snaith H., Sohrin Y., Sohst B., Sonke J. E., Speich S., Steinfeldt R., Stewart G., Stichel T., Stirling C. H., Stutsman J., Swarr G. J., Swift J. H., Thomas A., Thorne K., Till C. P., Till R., Townsend A. T., Townsend E., Tuerena R., Twining B. S., Vance D., Velazquez S., Venchiarutti C., Villa-Alfageme M., Vivancos S. M., Voelker A. H. L., Wake B., Warner M. J., Watson R., van Weerlee E., Alexandra Weigand M., Weinstein Y., Weiss D., Wisotzki A., Woodward E. M. S., Wu J., Wu Y., Wuttig K., Wyatt N., Xiang Y., Xie R. C., Xue Z., Yoshikawa H., Zhang J., Zhang P., Zhao Y., Zheng L., Zheng X. Y., Zieringer M., Zimmer L. A., Ziveri P., Zunino P. and Zurbrück C. (2018) The GEOTRACES Intermediate Data Product 2017. *Chem. Geol.* **493**, 210–223.

- Shiel A. E., Weis D. and Orians K. J. (2010) Evaluation of zinc, cadmium and lead isotope fractionation during smelting and refining. *Sci. Total Environ.* **408**, 2357–2368.
- Shiller A. M. and Boyle E. A. (1991) Trace elements in the Mississippi River Delta outflow region: Behavior at high discharge. *Geochim. Cosmochim. Acta* **55**, 3241–3251.
- Siebert C., Nägler T. F. and Kramers J. D. (2001) Determination of molybdenum isotope fractionation by double-spike multicollector inductively coupled plasma mass spectrometry. *Geochemistry, Geophys. Geosystems* **2**, 1032.
- Singer P. C. and Strumm W. (1970) Acidic Mine Drainage: The Rate Determining Step. *Science* (80- ). **167**, 1121–1124.
- Sivry Y., Riotte J., Sonke J. E., Audry S., Schäfer J., Viers J., Blanc G., Freydier R. and Dupré B. (2008) Zn isotopes as tracers of anthropogenic pollution from Zn-ore smelters The Riou Mort-Lot River system. *Chem. Geol.* **255**, 295–304.
- Skierszkan E. K., Mayer K. U., Weis D. and Beckie R. D. (2016) Molybdenum and zinc stable isotope variation in mining waste rock drainage and waste rock at the Antamina mine, Peru. *Sci. Total Environ.* **550**, 103–113.
- Sonke J. E., Sivry Y., Viers J., Freydier R., Dejonghe L., André L., Aggarwal J. K., Fontan F. and Dupré B. (2008) Historical variations in the isotopic composition of atmospheric zinc deposition from a zinc smelter. *Chem. Geol.* **252**, 145–157.
- Souto-Oliveira C. E., Babinski M., Araújo D. F. and Andrade M. F. (2018) Multi-isotopic fingerprints (Pb, Zn, Cu) applied for urban aerosol source apportionment and discrimination. *Sci. Total Environ.* **626**, 1350–1366.
- de Souza Machado A. A., Spencer K., Kloas W., Toffolon M. and Zarfl C. (2016) Metal fate and effects in estuaries: A review and conceptual model for better understanding of toxicity. *Sci. Total Environ.* **541**, 268–281.
- Spehar R. L., Anderson R. L. and Fiandt J. T. (1978) Toxicity and bioaccumulation of cadmium and lead in aquatic invertebrates. *Environ. Pollut.* **15**, 195–208.
- Strauss G. K., Madel J. and Alonso F. F. (1977) Exploration Practice for Strata-Bound Volcanogenic Sulphide Deposits in the Spanish-Portuguese Pyrite Belt: Geology, Geophysics, and Geochemistry. *Time- Strat. Ore Depos.*, 55–93.
- Szynkiewicz A. and Borrok D. M. (2016) Isotope variations of dissolved Zn in the Rio Grande watershed, USA: The role of adsorption on Zn isotope composition. *Earth Planet. Sci. Lett.* **433**, 293–302.
- Tornos F. (2006) Environment of formation and styles of volcanogenic massive sulfides: The Iberian Pyrite Belt. *Ore Geol. Rev.* **28**, 259–307.
- Tornos F., Lopez Pamo E. and Sanchez España J. (2008) The Iberian Pyrite Belt ed. Á. García-Cortés. *Inst. Geológico Y Min. España*, 1-31 pp.
- Torre B. M., Borrero-Santiago A. R., Fabbri E. and Guerra R. (2019) Trace metal levels and toxicity in the Huelva Estuary (Spain): A case study with comparisons to historical levels from the past decades. *Environ. Chem. Ecotoxicol.* **1**, 12–18.
- Twining B. S. and Baines S. B. (2013) The Trace Metal Composition of Marine Phytoplankton. *Ann. Rev. Mar. Sci.* **5**, 191–215.
- Vance D., Little S. H., Archer C., Cameron V., Andersen M. B., Rijkenberg M. J. A. and Lyons T. W. (2016) The oceanic budgets of nickel and zinc isotopes: the importance of sulfidic environments as illustrated

- Vig K., Megharaj M., Sethunathan N. and Naidu R. (2003) Bioavailability and toxicity of cadmium to microorganisms and their activities in soil: a review. *Adv. Environ. Res.* **8**, 121–135.
- Wang L., Guo J., Tsang D. C. W. and Hou D. (2023) Cadmium isotope fractionation during sorption to soil minerals: Lab evidence and field implication. *Chem. Geol.* **634**, 121607.
- Wang W., Chen M., Guo L. and Wang W. X. (2017) Size partitioning and mixing behavior of trace metals and dissolved organic matter in a South China estuary. *Sci. Total Environ.* **603–604**, 434–444.
- Wang Z. L. and Liu C. Q. (2003) Distribution and partition behavior of heavy metals between dissolved and acid-soluble fractions along a salinity gradient in the Changjiang Estuary, eastern China. *Chem. Geol.* **202**, 383–396.
- Wanty R. B., De Giudici G., Onnis P., Rutherford D., Kimball B. A., Podda F., Cidu R., Lattanzi P. and Medas D. (2013) Formation of a Low-Crystalline Zn-Silicate in a Stream in SW Sardinia, Italy. *Procedia Earth Planet. Sci.* **7**, 888–891.
- Wasylenki L. E., Swihart J. W. and Romaniello S. J. (2014) Cadmium isotope fractionation during adsorption to Mn oxyhydroxide at low and high ionic strength. *Geochim. Cosmochim. Acta* **140**, 212–226.
- Wiederhold J. G. (2015) Metal stable isotope signatures as tracers in environmental geochemistry. *Environ. Sci. Technol.* **49**, 2606–2624.
- Wilkinson J. J., Weiss D. J., Mason T. F. D. and Coles B. J. (2005) Zinc isotope variation in hydrothermal systems: Preliminary evidence from the Irish midlands ore field. *Econ. Geol.* **100**, 583–590.
- Wombacher F., Rehkämper M., Mezger K. and Münker C. (2003) Stable isotope compositions of cadmium in geological materials and meteorites determined by multiple-collector ICPMS. *Geochim. Cosmochim. Acta* **67**, 4639–4654.
- Wright D. A. and Welbourn P. M. (1994) Cadmium in the aquatic environment: A review of ecological, physiological, and toxicological effects on biota. *Environ. Rev.* **2**, 187–214.
- Wyatt N. J., Milne A., Woodward E. M. S., Rees A. P., Browning T. J., Bouman H. A., Worsfold P. J. and Lohan M. C. (2014) Biogeochemical cycling of dissolved zinc along the GEOTRACES `South Atlantic transect GA10 at 40°S. *Global Biogeochem. Cycles* **28**, 44–56.
- Xue Z., Rehkämper M., Schönbacher M., Statham P. J. and Coles B. J. (2012) A new methodology for precise cadmium isotope analyses of seawater. *Anal. Bioanal. Chem.* **402**, 883–893.
- Yan X., Zhu M., Li W., Peacock C. L., Ma J., Wen H., Liu F., Zhou Z., Zhu C. and Yin H. (2021) Cadmium Isotope Fractionation during Adsorption and Substitution with Iron (Oxyhydr)oxides. *Environ. Sci. Technol.* **55**, 11601–11611.
- Yang J., Li Y., Liu S., Tian H., Chen C., Liu J. and Shi Y. (2015) Theoretical calculations of Cd isotope fractionation in hydrothermal fluids. *Chem. Geol.* **391**, 74–82.
- Yang W. J., Ding K. B., Zhang P., Qiu H., Cloquet C., Wen H. J., Morel J. L., Qiu R. L. and Tang Y. T. (2019) Cadmium stable isotope variation in a mountain area impacted by acid mine drainage. *Sci. Total Environ.* **646**, 696–703.
- Yin N. H., Sivry Y., Benedetti M. F., Lens P. N. L. and van Hullebusch E. D. (2016) Application of Zn isotopes in environmental impact assessment of Zn–Pb metallurgical industries: A mini review. *Appl. Geochemistry* **64**, 128–135.
- Yin X., Wei R., Chen H., Zhu C., Liu Y., Wen H., Guo Q. and Ma J. (2021) Cadmium isotope constraints on heavy metal sources in a riverine system impacted by multiple anthropogenic activities. *Sci. Total Environ.* **750**, 141233.

Zhang Y., Planavsky N. J., Zhao M., Isson T., Asael D., Wang C. and Wang F. (2021) The isotopic composition of sedimentary organic zinc and implications for the global Zn isotope mass balance. *Geochim. Cosmochim. Acta* **314**, 16–26.

Zhang Y., Wen H., Zhu C., Fan H., Luo C., Liu J. and Cloquet C. (2016) Cd isotope fractionation during simulated and natural weathering. *Environ. Pollut.* **216**, 9–17.

Zhao Y., Vance D., Abouchami W. and de Baar H. J. W. (2014) Biogeochemical cycling of zinc and its isotopes in the Southern Ocean. *Geochim. Cosmochim. Acta* **125**, 653–672.

Zhong Q., Yin M., Zhang Q., Beiyuan J., Liu J., Yang X., Wang J., Wang L., Jiang Y., Xiao T. and Zhang Z. (2021) Cadmium isotopic fractionation in lead-zinc smelting process and signatures in fluvial sediments. *J. Hazard. Mater.* **411**, 125015.

Zhu C. W., Wen H. J., Zhang Y. X., Fan H. F., Fu S. H., Xu J. and Qin T. R. (2013) Characteristics of Cd isotopic compositions and their genetic significance in the lead-zinc deposits of SW China. *Sci. China Earth Sci.* **56**, 2056–2065.

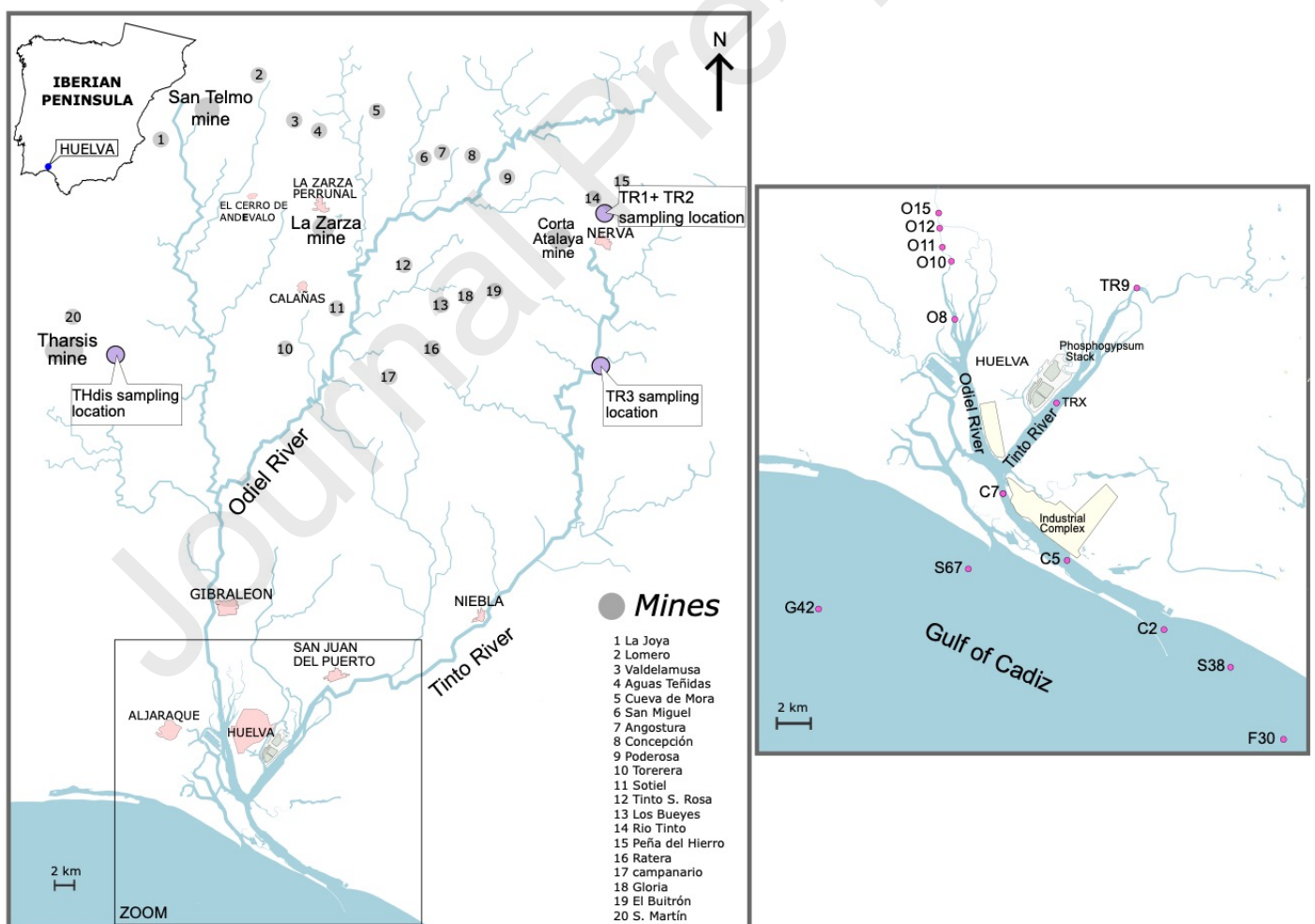


**Figure 1.** Left: location of water sampling locations in the Odiel and Tinto River watersheds. Right: Zoom of Huelva region to show water sampling locations in the Ria of Huelva estuary and the Gulf of Cadiz. Some local towns are indicated in pink, the industrial complexes in the region are coloured yellow and the grey circles mark the main mine localities (not an exhaustive list).

Journal Pre-proofs



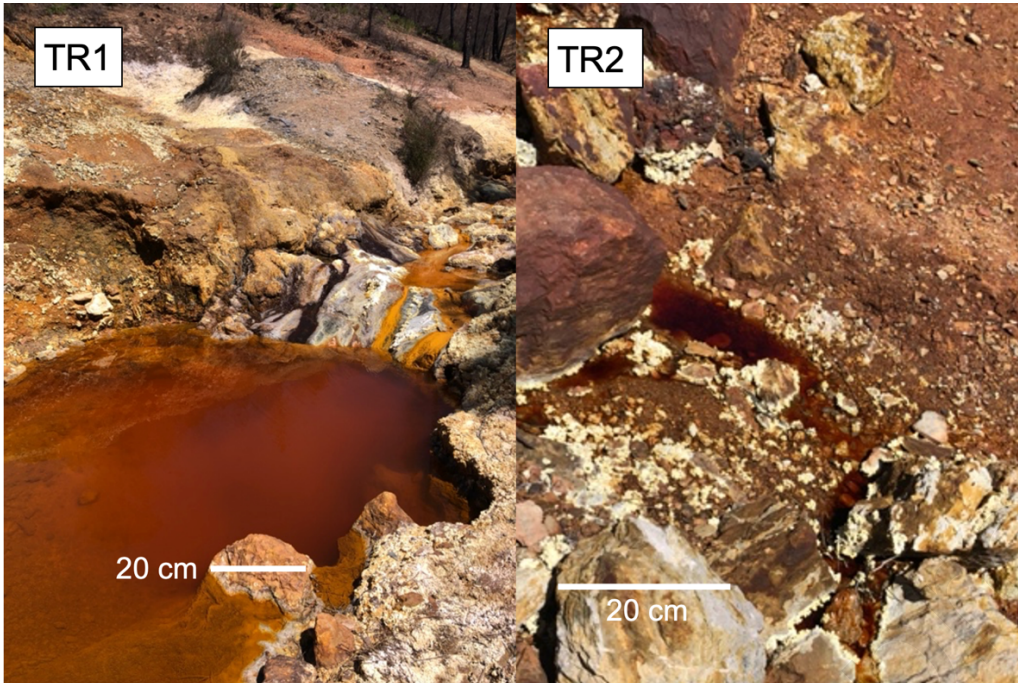


**Figure 2.** Photographs of the sampling locations of TR1 and TR2, showing distinctive impact of AMD (dark red colour) at TR2 compared to the lighter orange at TR1, indicative of schwertmannite precipitation.

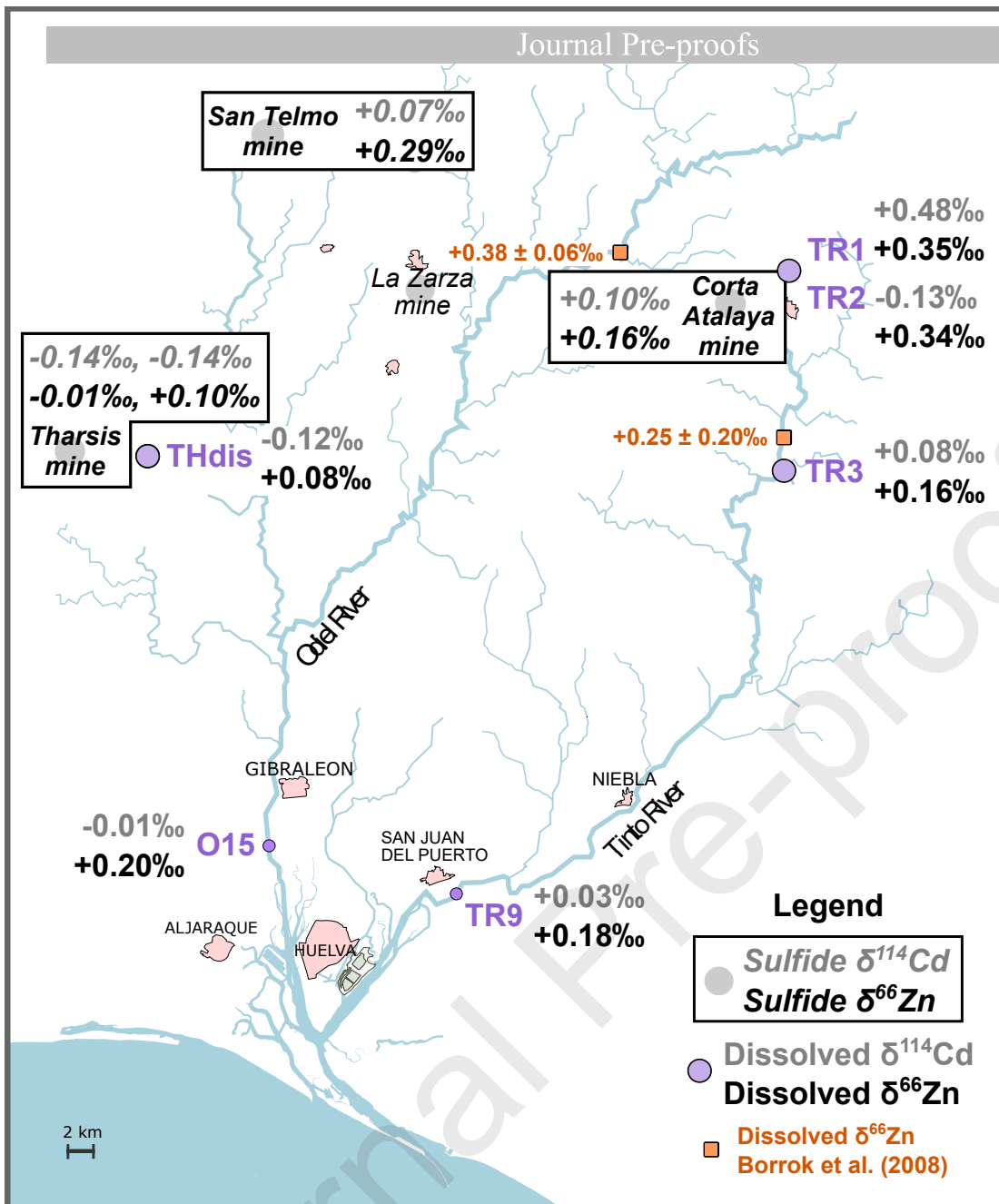


**Figure 3.**  $\delta^{114}\text{Cd}$  (grey text) and  $\delta^{66}\text{Zn}$  (black text) values of selected samples collected in the Odiel and Tinto watersheds in 2019. Boxed  $\delta$ -values in bold-italic font are for digests of mine sulfide samples.  $\delta$ -values in bold font are for dissolved phase water samples. Orange squares and values give the locations and  $\delta^{66}\text{Zn}$  values of water samples reported in Borrok et al. (2008).

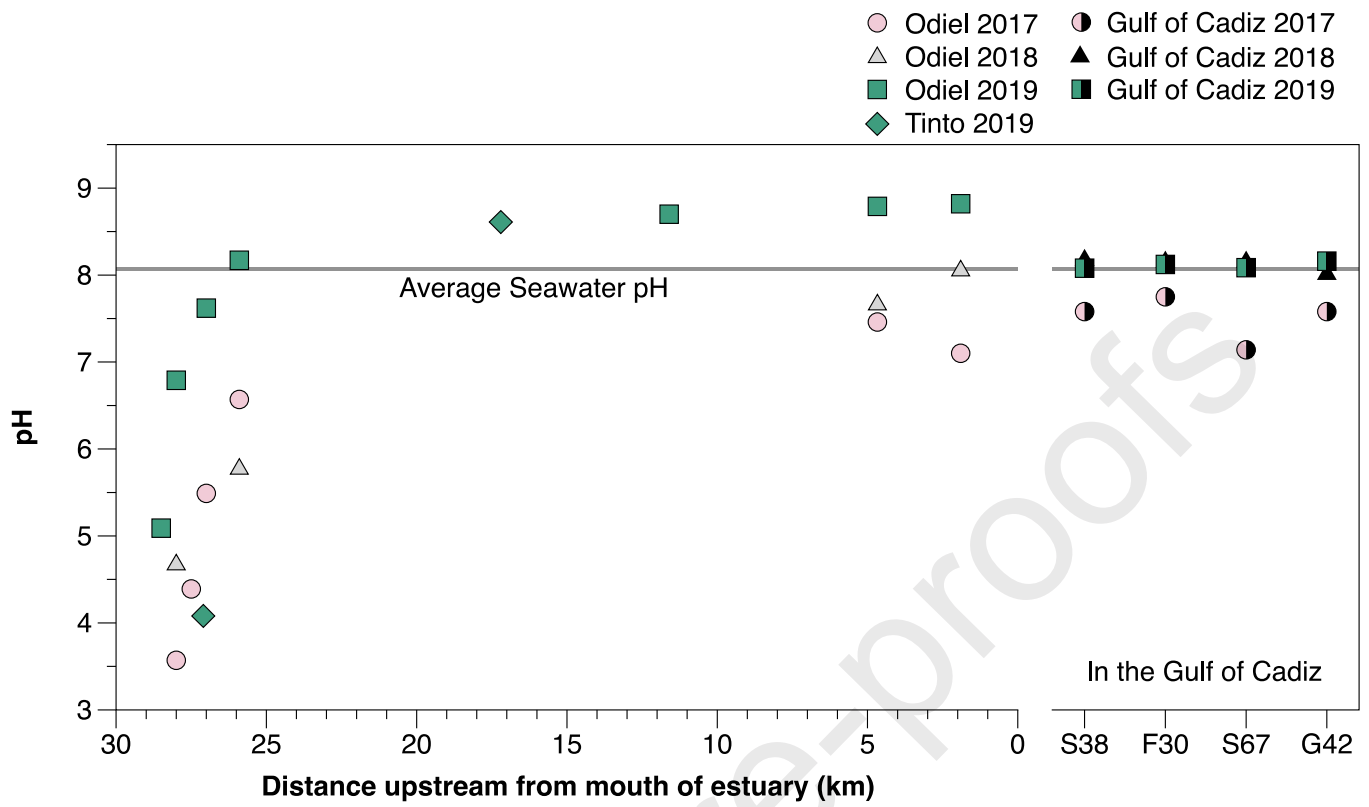


**Figure 4.** pH plotted against distance upstream from the mouth of the Ria of Huelva estuary and for the Gulf of Cadiz in 2017, 2018 and 2019.

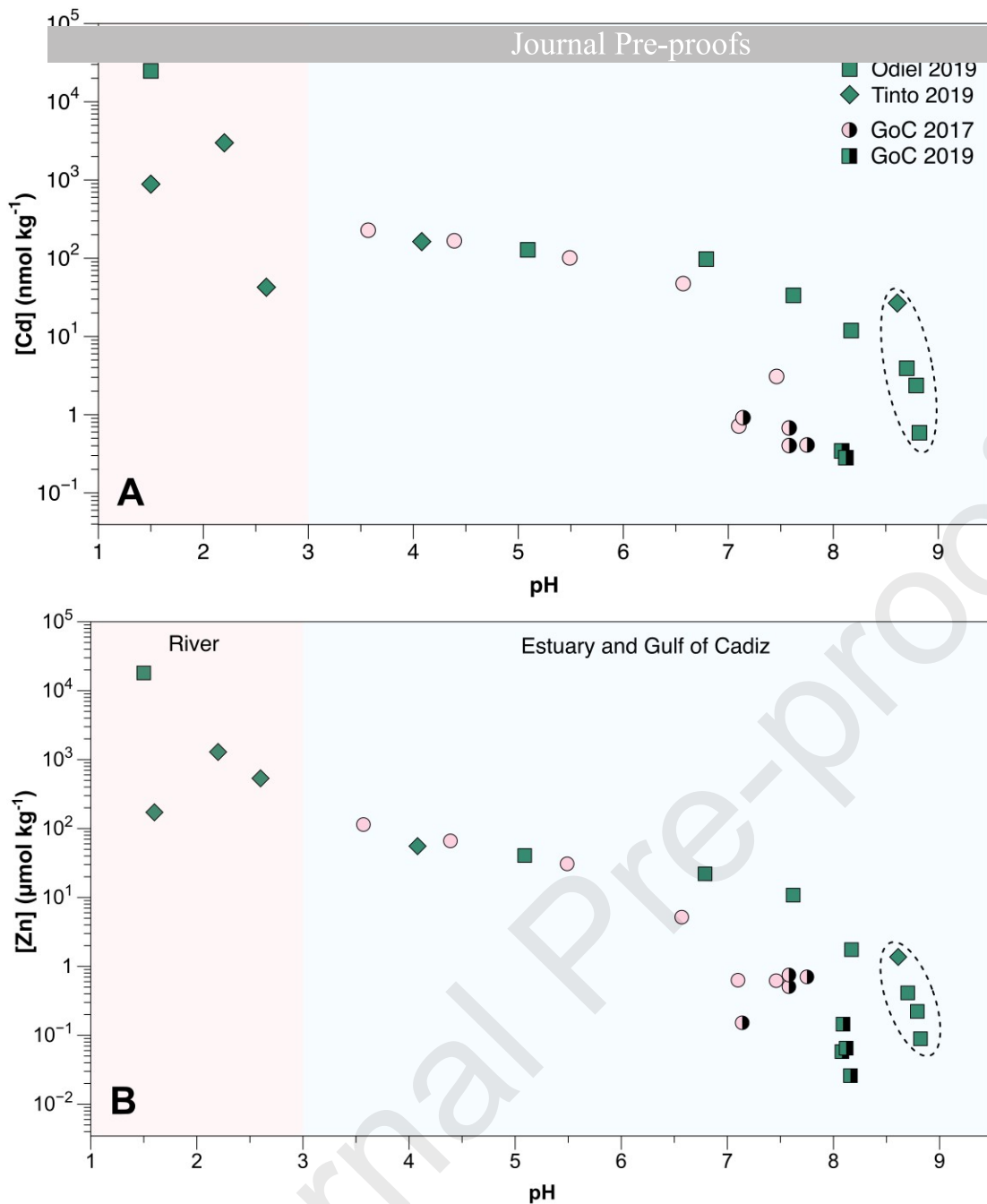


**Figure 5.** Dissolved Cd (Panel A) and dissolved Zn (Panel B) concentrations against pH for the Odiel and Tinto River watersheds (orange shaded background) and for the Ria of Huelva estuary and Gulf of Cadiz (blue shaded background), for samples collected in May 2017 and June 2019. Samples from the Gulf of Cadiz (GoC) are those with symbols divided in half. Samples from the confluence of the estuary are included in the 'Odiel' datasets. The 'Tinto' samples include waters collected in the Tinto River and Tinto branch of the Ria of Huelva estuary. Circled datapoints are 2019 estuarine samples with pH values more alkaline than Gulf of Cadiz seawater (see text for discussion).

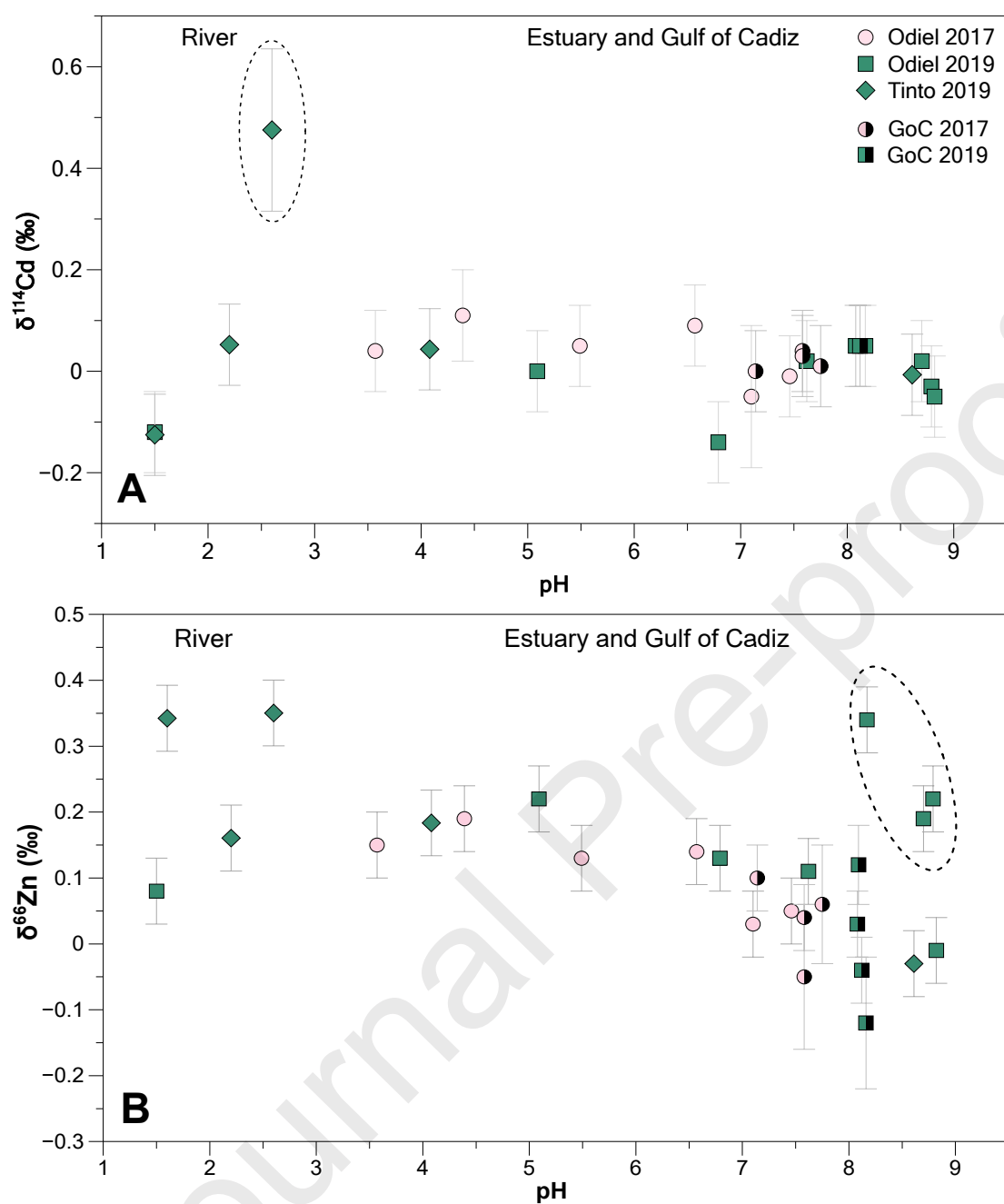


**Figure 6.** Cd (Panel A) and Zn (Panel B) isotope compositions plotted against pH for the water samples collected in 2017 and 2019. Colour shading and symbols are as in Figure 5. Samples from the confluence of the estuary are included in the 'Odiel' datasets. The 'Tinto' samples include waters collected in the Tinto River and Tinto branch of the Ria of Huelva estuary. Samples with anomalous  $\delta^{114}\text{Cd}$  and  $\delta^{66}\text{Zn}$  values are circled (see text for discussion).

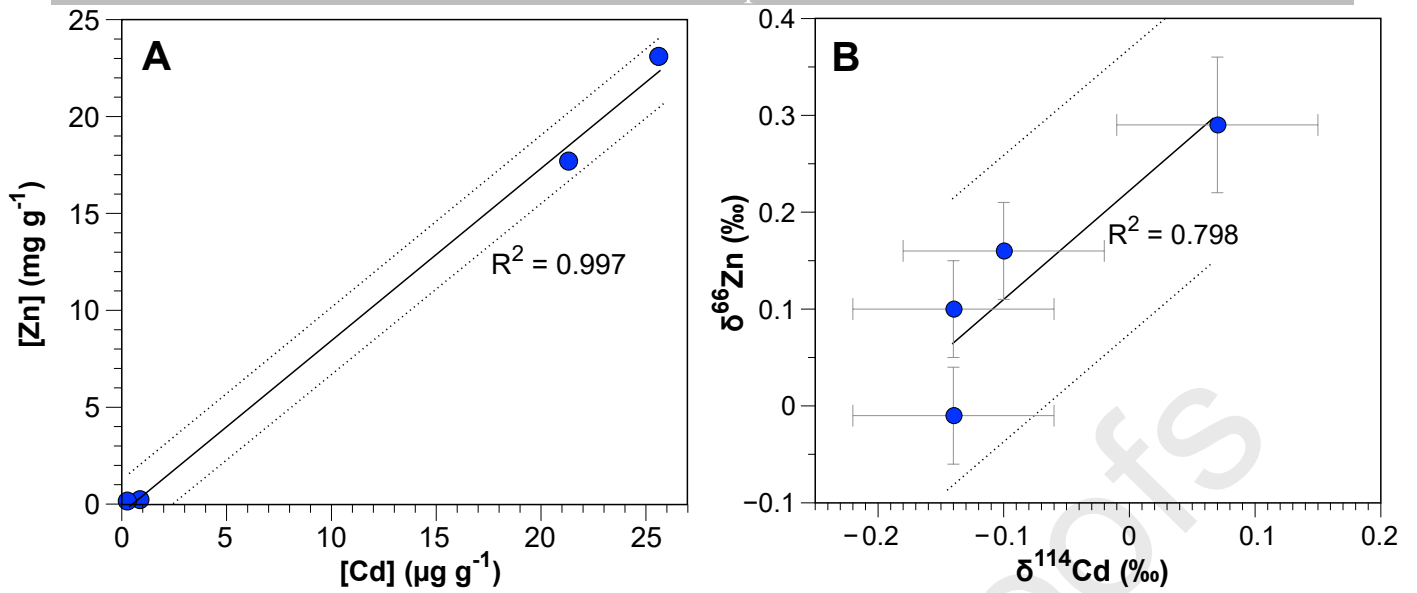


**Figure 7.** Cross plots of concentration and isotopic data for mine sulfide rock samples. Panel A: Cd concentration versus Zn concentrations. Panel B:  $\delta^{114}\text{Cd}$  and  $\delta^{66}\text{Zn}$  values. The data are for four sulfide samples from the mines Tharsis (two samples), Corta Atalaya and San Telmo (TH1, TH2, CA, ST). Linear regression lines and 95% confidence intervals are shown for reference.

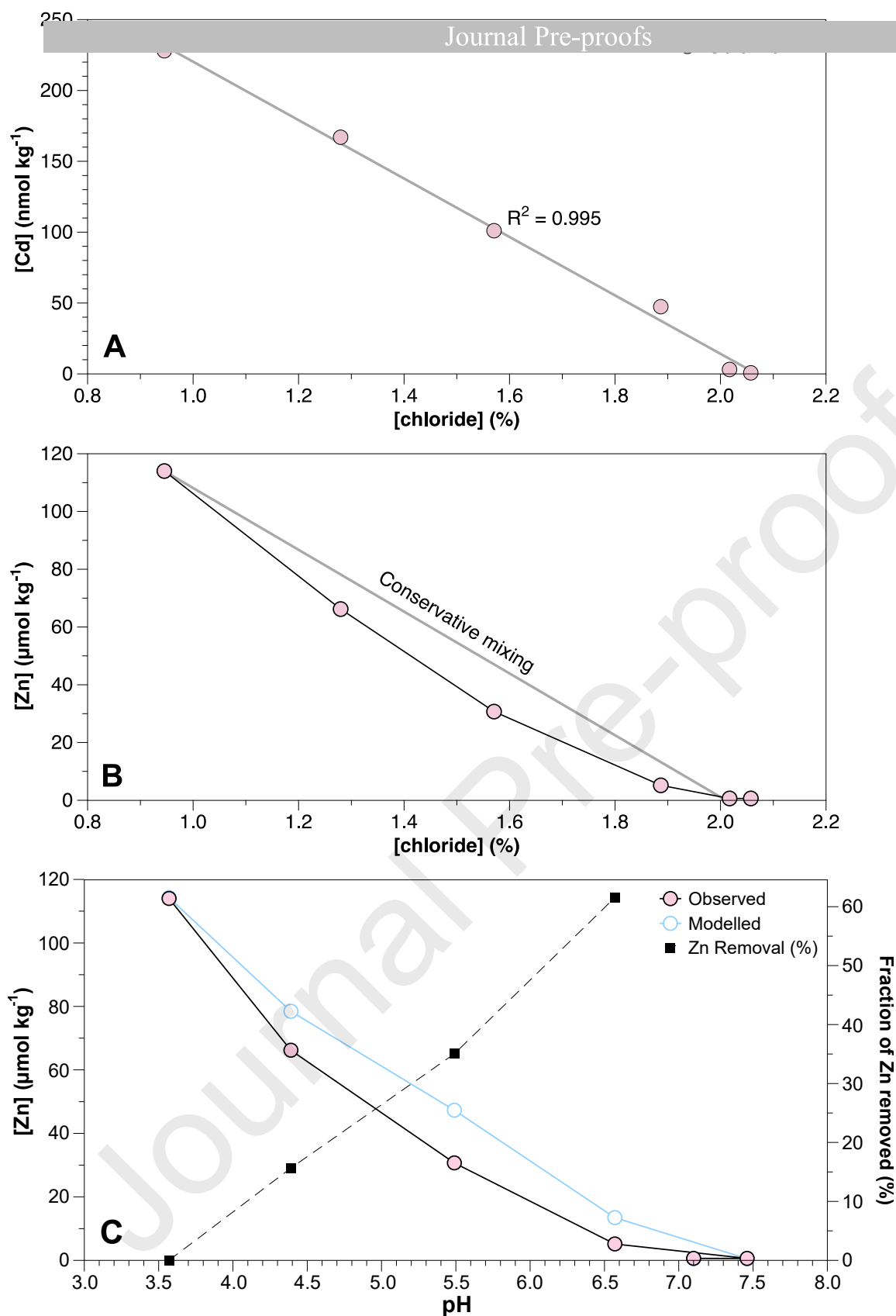


**Figure 8.** The behaviour of Cd and Zn in the Odiel branch of the Ria of Huelva estuary in 2017. Panel A: Cd (black line, pink circles) versus chloride concentrations with a linear regression function (grey line) including  $R^2$  value, illustrating conservative behaviour of Cd in the estuary in 2017. Panel B: Zn versus chloride concentrations, showing non-conservative behaviour of Zn in the estuary in 2017. Panel C: Zn concentrations versus pH compared to modelled Zn concentrations assuming conservative behaviour (blue line, open circles). Also shown is the modelled fraction of Zn removed from the dissolved phase (dashed black line, see text for discussion).

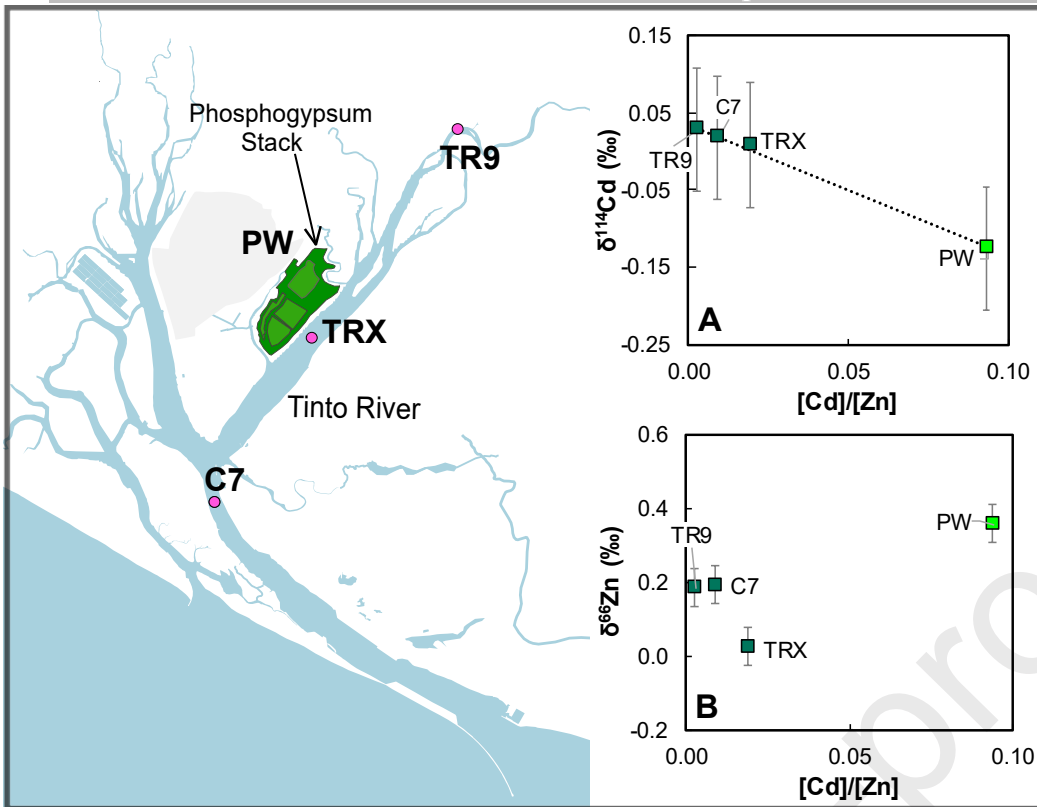


**Figure 9.** Map of the Ria of Huelva estuary showing the location of the phosphogypsum stack and locations of relevant samples. PW refers to process water, which is the solution sitting on the surface of the phosphogypsum stack (coloured in a lighter green). Inset graphs show dissolved  $\delta^{114}\text{Cd}$  (Panel A) and  $\delta^{66}\text{Zn}$  (Panel B) versus the ratio of dissolved Cd/Zn concentration. Dashed line on Panel A shows a linear regression, showing the likely impact of Cd contamination from the phosphogypsum stack on Cd/Zn ratios and  $\delta^{114}\text{Cd}$  values in the estuary.



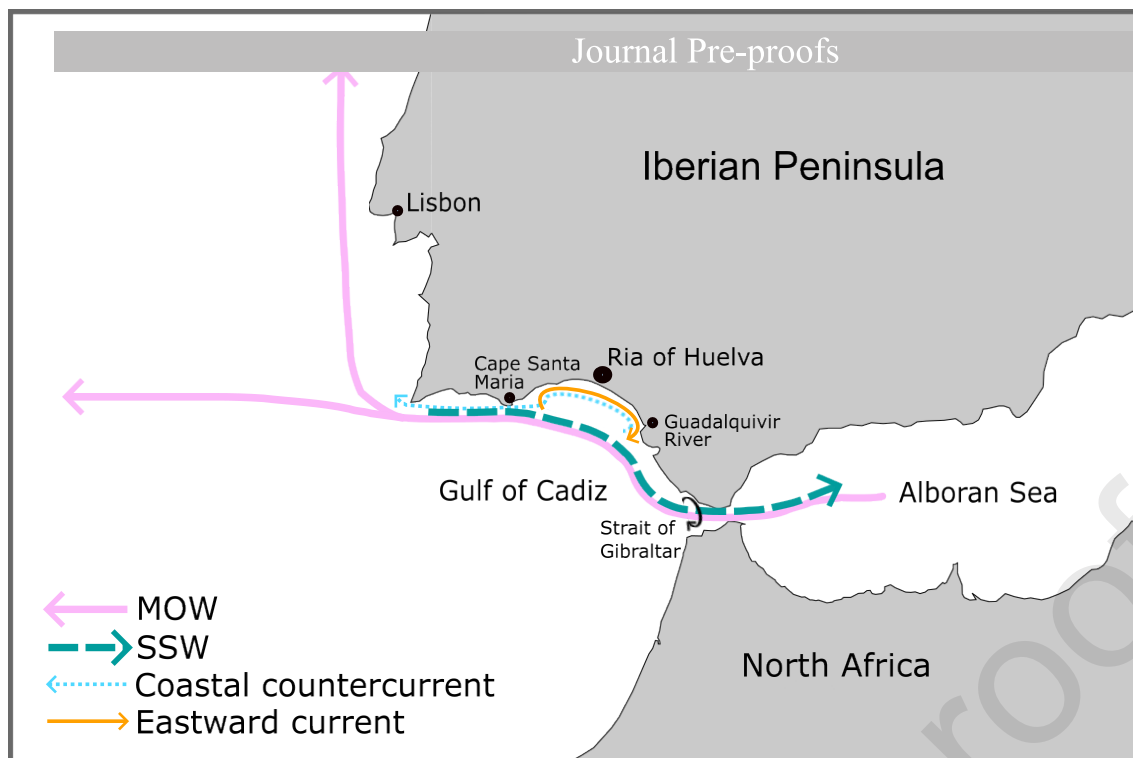


**Figure 10.** Schematic representation of relevant currents in the Gulf of Cadiz. Spanish Shelf Water (SSW) is a surface current, whilst the flow of Mediterranean Outflow Water (MOW) is at depths of 400 m in the Gulf of Cadiz and sinks to between 500 and 1500 m along the western coast of the Iberian Peninsula. The black curly arrow in the Strait of Gibraltar demonstrates proposed coupling between the inflow and outflow water masses (Peliz *et al.*, 2009).

**Table 1.** Summary of the Cd and Zn isotope compositions and concentrations determined for GEOTRACES samples in this study and reported in the literature.

		$\delta^{114}\text{Cd} (\text{‰}) \pm 2 \text{ SD}$	$[\text{Cd}] \text{ (nmol kg}^{-1}\text{)}$	Yield (%)		$\delta^{66}\text{Zn} (\text{‰}) \pm 2 \text{ SD}$	$[\text{Zn}] \text{ (nmol kg}^{-1}\text{)}$	Yield (%)
GDI	<i>This study</i>	$0.44 \pm 0.08$	0.24	90	<i>This study</i>	$0.36 \pm 0.05$	2.01	117
	Boyle <i>et. al.</i> 2012	$0.47 \pm 0.04$	0.27		Conway and John, 2014 <sup>a</sup>	$0.38 \pm 0.03$	1.71	
1962	<i>This study</i>	$0.27 \pm 0.08$	0.56	96				
	Bryan <i>et. al.</i> 2021	$0.28 \pm 0.12$	0.58					
2268	<i>This study</i>	$0.26 \pm 0.08$	0.64	97	<i>This study</i>	$0.50 \pm 0.05$	6.02	94

<sup>a</sup>Station 10 of GEOTRACES GA03 transect at 31.75 °N 64.17 °W

<sup>b</sup>GEOTRACES intermediate data product: Schlitzer et al. (2017)

Journal Pre-proofs

**Table 2.** Cd and Zn isotope compositions and concentrations, chloride concentrations pH, Eh, and electrical conductivity (EC) for samples from the Huelva region.

Sample	Chloride (%)	pH	EC (mS/cm)	Eh (mV)	[Cd] (nmol kg <sup>-1</sup> )	$\delta^{114}\text{Cd}$ (‰)	2 SD	[Zn] ( $\mu\text{mol kg}^{-1}$ )	$\delta^{66}\text{Zn}$ (‰)	2 SD
<u>Ria of Huelva estuary, May 2017</u>										
O12-17	0.95	3.57			228	0.04	0.08	114	0.15	0.05
O11-17	1.28	4.39			167	0.08	0.09	66.2	0.19	0.05
O10-17	1.57	5.49			101	0.05	0.08	30.7	0.13	0.05
O8-17	1.89	6.57			47.4	0.10	0.08	5.17	0.14	0.05
C5-17	2.02	7.46			3.08	-0.01	0.08	0.618	0.05	0.05
C2-17	2.06	7.10			0.717	-0.05	0.14	0.625	0.03	0.05
<u>Gulf of Cadiz seawater, May 2017</u>										
S38-17	1.91	7.58			0.676	0.04	0.08	0.508	0.04	0.05
F30-17		7.75			0.410	0.01	0.08	0.704	0.06	0.09
S67-17	2.09	7.14			0.915	0.00	0.08	0.152	0.10	0.05
G42-17	2.02	7.58			0.403	0.03	0.08	0.750	-0.05	0.11

---

Stream or river waters, June 2019

TR1	2.6			42.6	0.48	0.16	172	0.35	0.05
TR2	1.5			885	-0.13	0.08	535	0.34	0.05
TR3	2.2			2990	0.08	0.08	1290	0.16	0.05
THdis	2.1			24800	-0.12	0.08	18100	0.08	0.05

---

Phosphogypsum stack, June 2019

PW	1.11	55.8	680	144000	-0.13	0.08	1530	0.35	0.05
----	------	------	-----	--------	-------	------	------	------	------

---

Ria of Huelva estuary, June 2019

TR9	2.21	4.08	52.1	565	163	0.03	0.08	55.5	0.18	0.05
TRX	2.62	8.61	59.8	360	26.7	0.01	0.08	1.37	0.02	0.05
O15-19	2.15	5.09	47.9	467	128	-0.01	0.08	40.6	0.20	0.05
O12-19	2.40	6.79	55.1	434	97.5	-0.14	0.08	22.0	0.17	0.05
O10-19	2.56	7.62	58.3	402	64.4	0.02	0.08	10.8	0.11	0.05
O8-19	2.74	8.17	61.1	421	20.4	0.05	0.08	1.75	0.34	0.05
C7-19	2.61	8.70	59.1	394	3.92	0.02	0.08	0.413	0.19	0.05
C5-19	2.59	8.79	58.7	384	2.36	-0.03	0.08	0.222	0.22	0.05

C2-19	2.59	8.82	58.3	371	0.588	-0.05	0.08	0.089	-0.01	0.05
<hr/>										
<u>Gulf of Cadiz seawater, June 2019</u>										
S38-19	2.55	8.08	58.2	452	0.344	0.05	0.08	0.058	0.03	0.05
F30-19	2.45	8.12	58.9	541	0.282	0.05	0.08	0.065	-0.04	0.05
S67-19		8.09	58.8	313				0.145	0.12	0.06
G42-19	2.31	8.16	59.2	323				0.026	-0.12	0.10
<hr/>										
<u>Sulfide rocks</u>										
CA					<u>0.956</u>	-0.10	0.08	<u>0.234</u>	0.16	0.05
TH1					<u>25.7</u>	-0.14	0.08	<u>23.1</u>	-0.01	0.05
TH2					<u>21.4</u>	-0.14	0.08	<u>17.7</u>	0.10	0.05
ST					<u>0.349</u>	0.07	0.08	<u>0.160</u>	0.29	0.07

*italics* = mg g<sup>-1</sup> for [Zn] and µg g<sup>-1</sup> for [Cd]

2 SD uncertainties are the long-term reproducibility of the relevant secondary standard (London Zn or BAM-I012) or of repeat analyses, whichever is larger, with the exception TR1 δ<sup>114</sup>Cd, for which the error is the 2 SD of multiple analyses of the primary standard during the measurement session.

**Table 3.** Zn isotope compositions and concentrations of the digested and leached particulates from samples O12-19 and C7-19 and two USGS rock reference materials

**Bulk digest**

**Leachate**

	$\delta^{66/64}\text{Zn}$ (‰)	2 SD	[Zn]	$\delta^{66/64}\text{Zn}$ (‰)	2 SD	[Zn]
			<u>*nmol L<sup>-1</sup></u>			<u>*nmol L<sup>-1</sup></u>
O12 19p	0.58	0.05	149	0.60	0.05	73.0
C7 19p	0.19	0.07	66.2	0.51	0.05	23.0
			<u><math>\mu\text{g g}^{-1}</math></u>			<u><math>\mu\text{g g}^{-1}</math></u>
BCR-2	0.32	0.05	141	0.81	0.05	2.84
Nod P1	0.79	0.05	1540	0.81	0.05	29.6

\*Units for the Huelva particulate samples are given in nmol L<sup>-1</sup> (i.e., nmol Zn per L of filtered water), because the sample mass is not known.

### Declaration of interests

The authors declare that they have no known competing financial interests or personal relationships that could have appeared to influence the work reported in this paper.

The authors declare the following financial interests/personal relationships which may be considered as potential competing interests:

Journal Pre-proofs